Electronic Supplementary Material (ESI) for ChemComm.

SUPPORTING INFORMATION

Red light-triggered nucleic acid-templated reaction based on cyclic oligonucleotide substrates

Oleksii Zozulia, Tobias Bachmann, Nina Deussner, Frank Beierlein, Mike Heilemann and Andriy Mokhir*

Content

Materials and Methods

Commercially available chemicals of the best quality were obtained from Aldrich/Sigma/Fluka (Germany) and used without additional purification. Standard phosphoramidites and solid supports for DNA solid phase synthesis were obtained from Aldrich (Germany) and 5'-DMT-dA(Bz) synthesis columns (1000 Å, 1μmol scale) - from Biosearch Technologies (USA). DNAs were synthesized using K&A H-8 DNA/RNA synthesizer. ^{1}H- and ^{13}C-NMR spectra were measured on a Bruker Avance 300. MALDI-TOF mass spectra were recorded on a Shimadzu Axima mass spectrometer. The matrix mixture (2:1 v/v) was prepared from 2′,4′,6′-trihydroxyacetophenone (THAP, 0.3 M solution in acetonitrile) and diammonium citrate (0.1 M in water). Samples for mass spectrometry were prepared by the dried droplet method using a 1:2 probe/matrix ratio. Mass accuracy with external calibration was 0.1% of the peak mass, which is ±9.0 at *m*/*z* 9000. HPLC was performed at 22 °C on a Shimadzu liquid chromatograph equipped with UV-visible (diode array) and fluorescence detectors and a Macherey–Nagel Nucleosil C18 250 × 4.6 mm column. Gradients of solution B (CH_3CN) in solution A (0.1 M aqueous (NEt_3H)(OAc)) were applied to purify conjugates. UV/Vis spectra of DNA conjugates were measured on a Lambda Bio+ UV/Vis spectrophotometer (Perkin Elmer) by using micro-cuvettes with a sample volume of 100 μL (BRAND GmbH, Germany). Fluorescence spectra were acquired on a Varian Cary Eclipse fluorescence spectrophotometer using fluorescence cuvettes (Hellma GmbH, Germany) with a sample volume of 1 mL. Irradiation experiments were performed with a LED Array 672 (λ = 650 nm) from Cetoni GmbH (Germany).

Synthesis of DNA conjugates

Conjugates ON2~P, ON3~3 and Q~ON4 were prepared as described previously.[1]

Synthesis of cyclic substrate cF-***L****-ON1

DNA precursors were prepared by the standard solid phase synthesis using commercially available DNA monomer phosphoramidites (dA-Bz, dC-Bz, dG-dmf, dT; Aldrich, Germany) and controlled pore glass (CPG) solid supports, which carry one of the protected nucleosides according to the manufacturer's recommendations. In all cases ~30-33 mg of CPG containing on its surface ~1 μmol of a protected nucleoside was used as a starting material.

Structures of building blocks **s1**-**s5** used in the synthesis of the cyclic DNA substrate cF-***L****-ON1 are shown in Scheme S1.

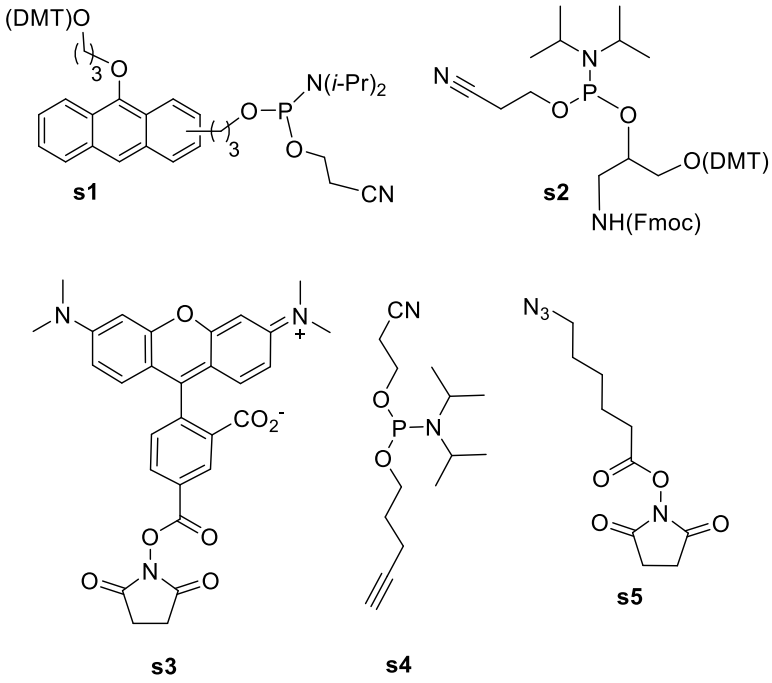

Scheme S1. Structures of building blocks used for the synthesis of cyclic substrate cF-***L****-ON1. These compounds were prepared by standard methods from common starting materials. Compound s1 was obtained as previously described.[1]

The synthesis of cF-***L****-ON1 is outlined in Scheme S2. First, a protected DNA strand 3'-ACCGTGGGTCGTGT was assembled on the solid support **s6** using standard solid phase synthesis and the terminal DMT-group was cleaved off (**s7**). Then, an internal trifluoroacetyl (Tfa)-protected primary amino-group was introduced by coupling commercially available amino-modifier C6-dT-CE phosphoramidite (Link Technologies, UK). In particular, the latter reagent was dissolved in anhydrous CH_3CN (final concentration 0.15 M volume 0.2 mL). Then just before coupling the solution of DCI (0.1 mL of 0.25 M solution in CH_3CN) was added and the resulting mixture was added to the DNA-containing solid support. After 15 minutes the solution was removed from CPGs and the latter one was washed with CH_3CN, treated with CAP A (acetic anhydride, 10% in THF) and CAP B (THF/N-methylimidazole: 84/16, v/v) mixture 1/1 (v/v) for 3 min and finally treated with the oxidizer solution (iodine in pyridine/water/THF, 0.41/9.05/90.54, v/v/v, 0.02 M) for 1 min. Next, the CPG was washed with CH_3CN, dried in vacuum (0.05 mbar) and the terminal DMT group was cleaved. Further on, another DNA strand 3'-ACTTCT was assembled and the terminal DMT group was cleaved to obtain **s8**.

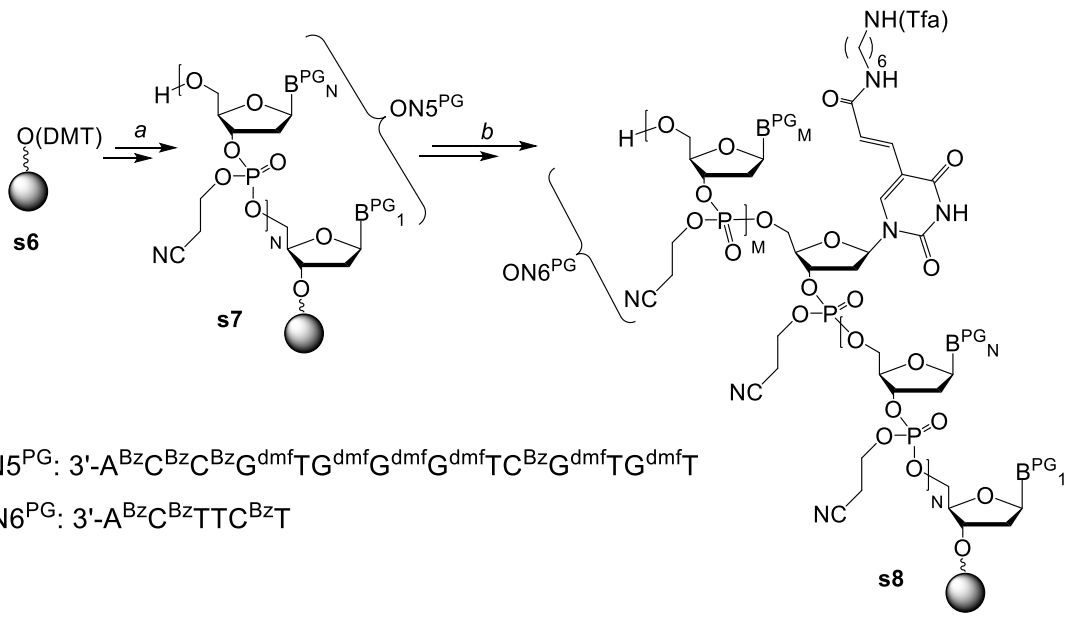

ON5^{PG}: 3'-A^{Bz}C^{Bz}C^{Bz}G^{dmf}TG^{dmf}G^{dmf}G^{dmf}TC^{Bz}G^{dmf}TG^{dmf}T

ON6^{PG}: 3'-A^{Bz}C^{Bz}TTC^{Bz}T

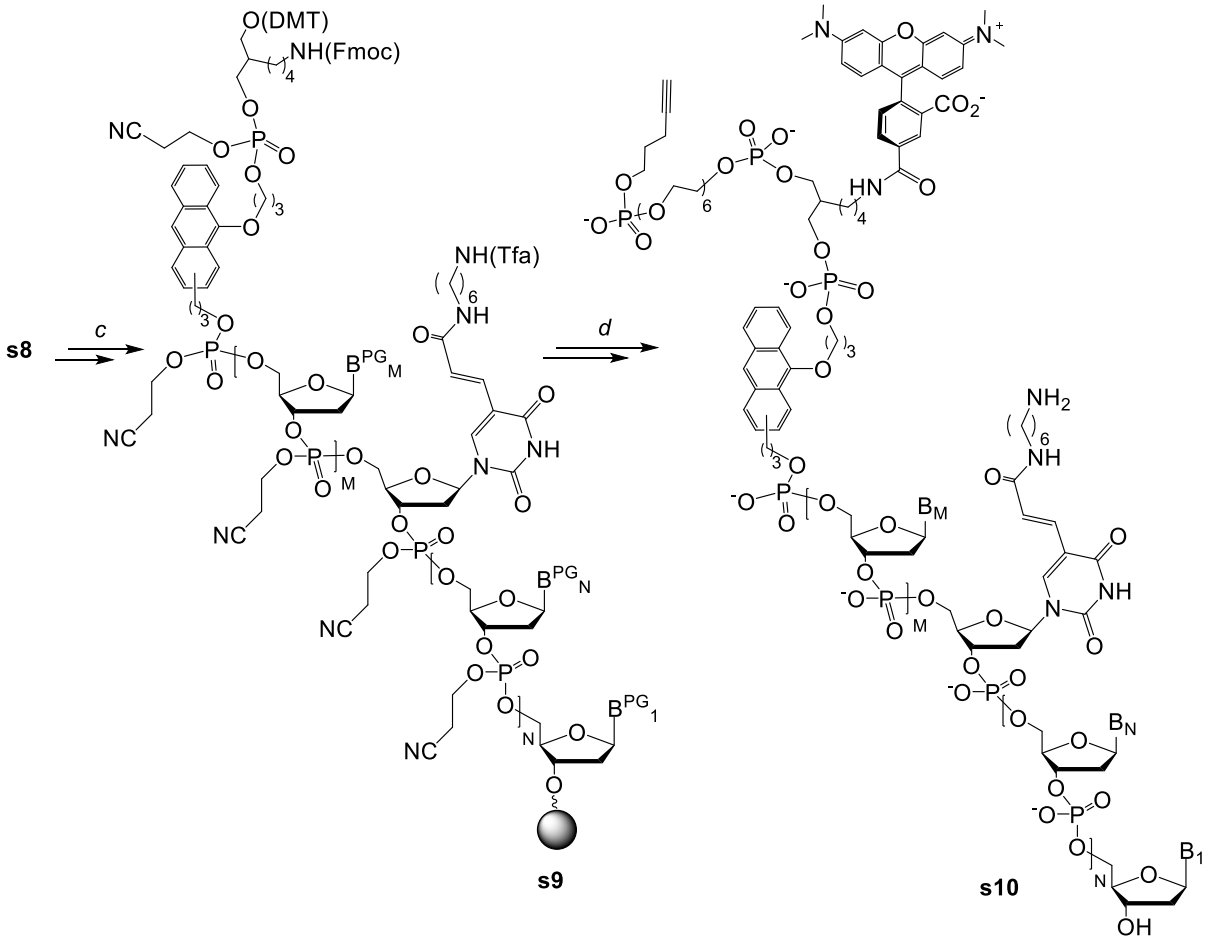

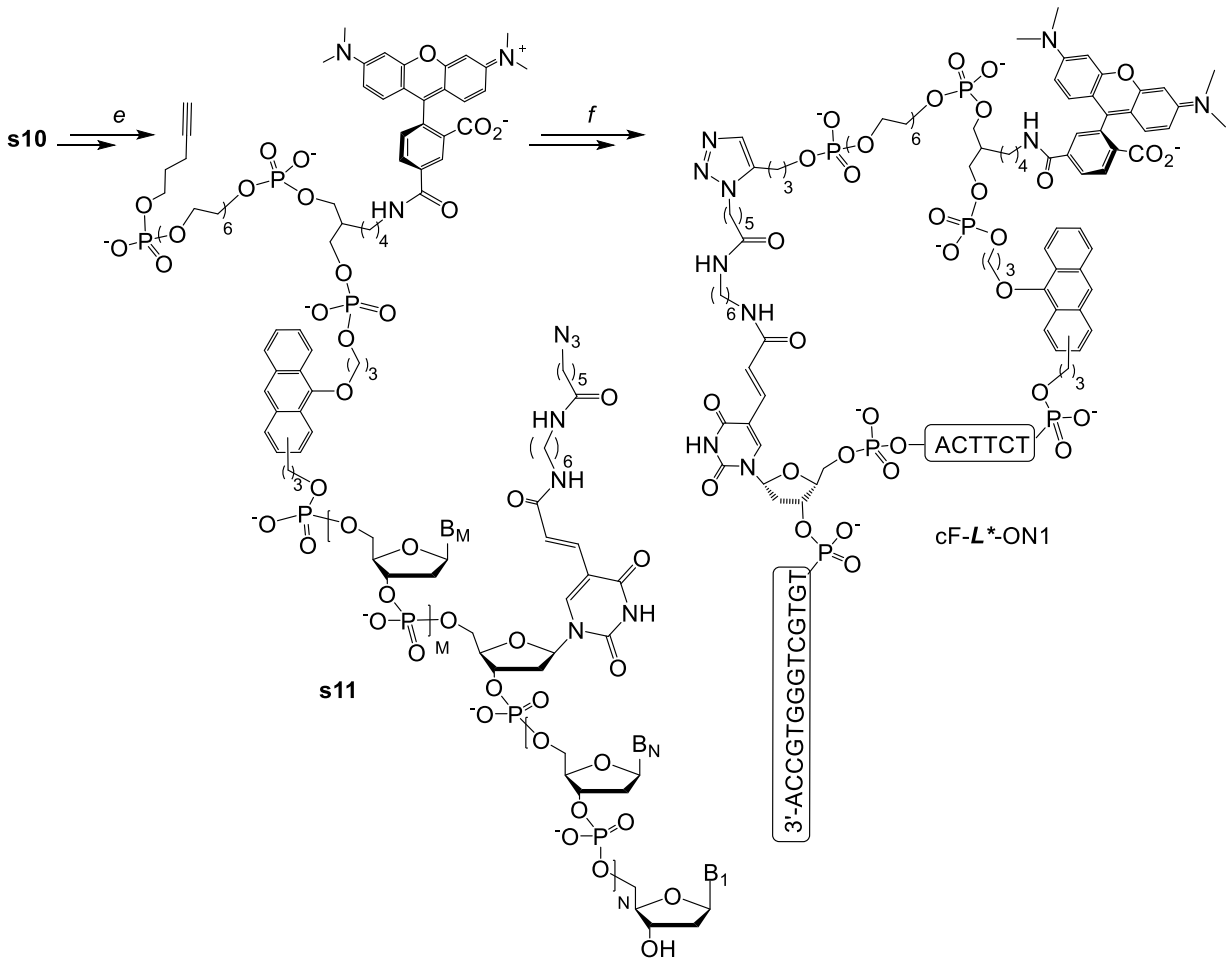

Scheme S2. Synthesis of a cyclic substrate cF-***L*******-ON1: (a) solid phase synthesis of an oligonucleotide strand (ON5) including cleavage of a terminal DMT group; (b) 1. amino-Modifier C6-dT-CE phosphoramidite (Link Technologies, UK), DCI in CH_3CN; 2. solid phase synthesis of an oligonucleotide (ON6) strand including cleavage of a terminal DMT group; (c) 1. Compound **s1** (Scheme S1) and DCI in CH_3CN; 2. acetic anhydride, N-methylimidazole in THF; 3. I_2, pyridine, H_2O, THF; 4. CCl_3CO_2H in CH_2Cl_2; 5-8: the same as steps 1-4, except that **s1** was replaced with **s2**; (d) 1. DBU in DMF; 2. Building block **s3**, DIPEA; 3. CCl_3CO_2H in CH_2Cl_2; 4-7. the same as steps c1-c4, except that **s1** was replaced with spacer-CE phosphoramidite 18 (HEG, Link Technologies, UK); 8-11. the same as steps c1-c4, except that **s1** was replaced phosphoramidite **s4**; 12. *t*-$BuNH_2$, H_2O, MeOH, 60 °C; (e) **s5**, Na_2HPO_4/NaH_2PO_4, pH 8.2; (f) $CuSO_4$, sodium ascorbate, THPTA ligand.

In the next step, phosphoramidite **s1** (Scheme S1) followed by phosphoramidite **s2** were sequentially coupled to **s8** analogously to the coupling of amino-Modifier C6-dT-CE

phosphoramidite described above to obtain **s9**. To attach a fluorophore to the DNA the fluorenylmethyloxycarbonyl (Fmoc)-protected amino group on **s9** was first deprotected by the treatment with DBU in DMF (2 %, v/v, 2 mL, 3 times, each time for 45 min). Than the CPG was washed with DMF (2x 2 mL), CH_3CN (2 mL) and dried *in vacuo* (0.05 mbar). Separately, building block **s3** (TMR-NHS ester, 100 µmol) was dissolved in DMF (1 mL) and DIPEA (38 µL, 220 mmol) was added that was followed by the addition of the CPG containing the deprotected amino-group. The slurry obtained was vortexed overnight, than the CPG was filtered, washed with DMF (3x1 mL), CH_3CN (1 mL) and dried *in vacuo* (0.05 mbar). Next, the DMT-group was cleaved off and phosphoramidites spacer-CE phosphoramidite 18 (HEG, Link Technologies, UK) and **s4** were coupled one after another as described above for other phosphoramidites. The obtained material was deprotected and the DNA conjugate was cleaved off from the solid support by treatment with a mixture of *tert*-butylamine/water/methanol (1/2/1, v/v/v) at 60°C for 16 h to obtain conjugate **s10**. The latter was purified by HPLC. Conjugate **s10** was dissolved in phosphate buffer (100 mM Na_2HPO_4/NaH_2PO_4, pH 8.2, 80 µL) to obtain its 270 µM solution. Reagent **s5** (5 eq, dissolved in DMSO, 10 µL) was added and the final mixture was mixed overnight at 22 °C. The resulting solution was diluted to 150 µL with water and purified by HPLC to obtain conjugate **s11**. Further, cyclization of **s11** was conducted analogously to the protocol reported elsewhere.[2] In particular, to 4000 µL of 0.2 M aqueous NaCl (degassed and additionally purged with argon), a tris(3-hydroxypropyltriazolylmethyl)amine (THPTA ligand, 22.6 µmol), sodium ascorbate (32.8 µmol), and $CuSO_4x5H_2O$ (3.28 µmol) were added sequentially. To the above solution, conjugate **s11** (16.4 nmol in 100 µL of water) was added (final concentration of 4 µM) and the resulting mixture was stored at room temperature for 2 h. The reaction mixture was quenched by addition of Na_2S (6 µmol in 100 µL of water), further desalted using a NAP-25 column (GE Healthcare) and then lyophilized. Resulting solid was re-dissolved in water and purified by HPLC leading to cF-***L****-ON1.

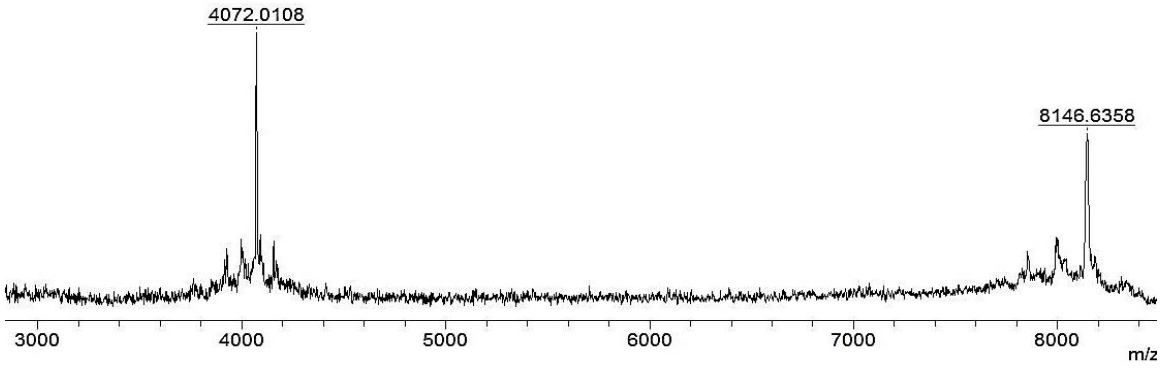

Figure **S1**. MALDI-TOF mass spectrum of conjugate **s11**.

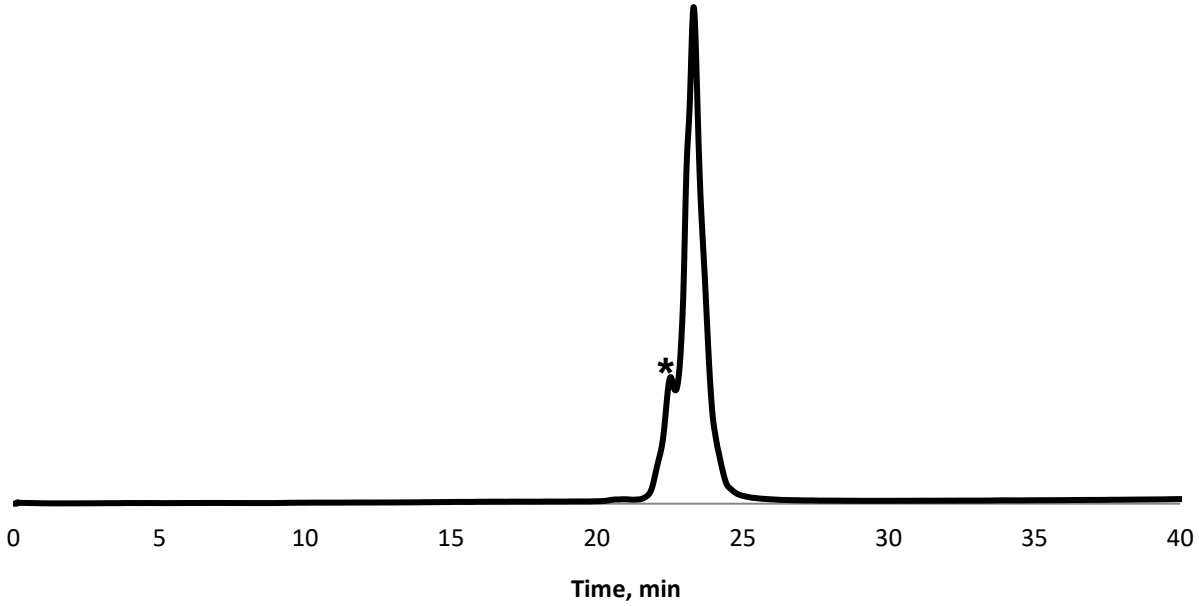

Figure **S2**. HPLC profile of conjugate **s11**. (*) – The product of spontaneous cyclization of **s11**.

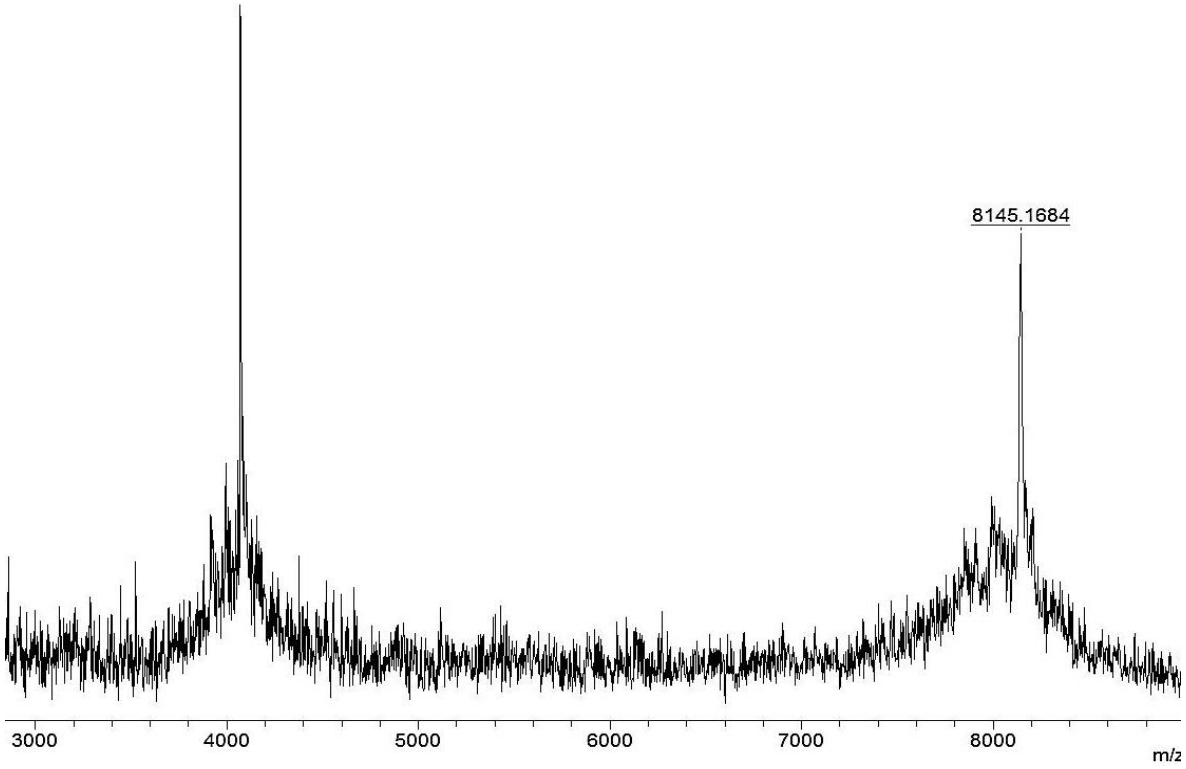

Figure **S3**. MALDI-TOF mass spectrum of cF-***L****-ON1, the product of cyclization of conjugate **s11**.

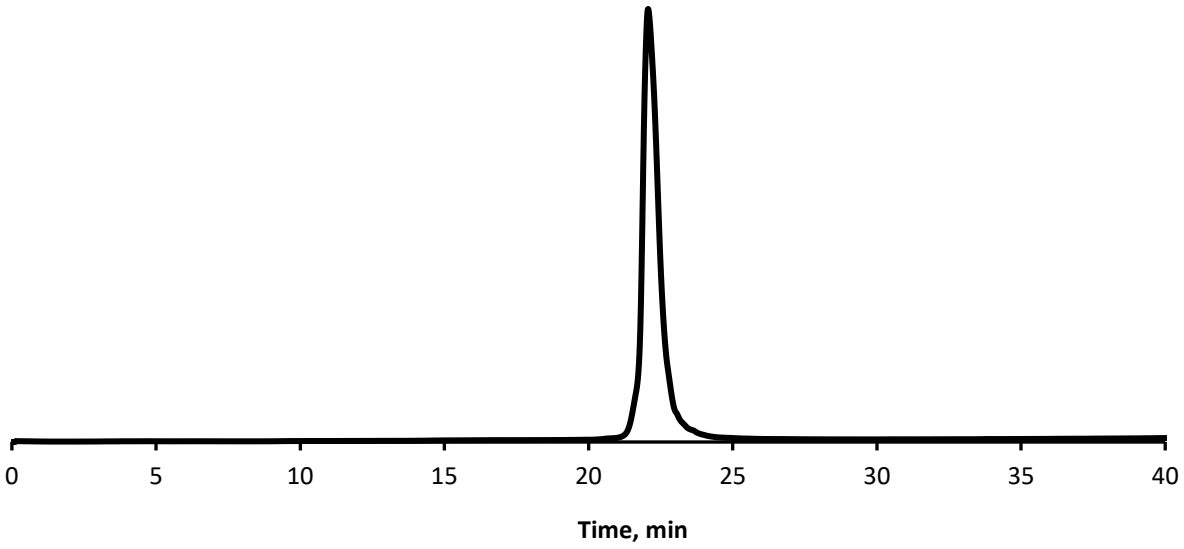

Figure **S4**. HPLC profile of cF-***L****-ON1.

*Study of $^1O_2$-mediated opening of the cyclic structure of cF-**L***-ON1*

The product of the reaction of cF-***L****-ON1 (*m/z* 8141 Da) with $^1O_2$ is expected to be acyclic and has higher molecular weight (Δm= 32 Da) than the initial compound (*m/z* 8173 Da, Scheme S3).

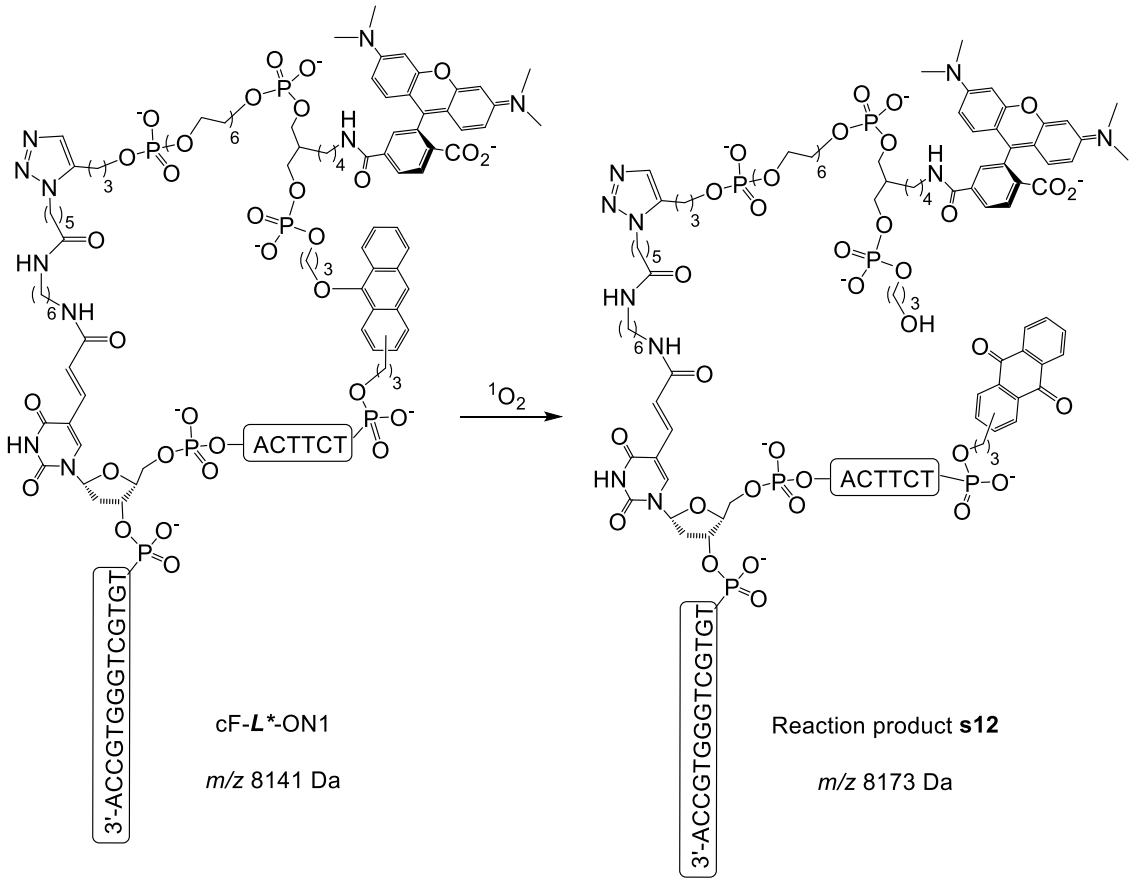

Scheme S3. An outline of the reaction of $^1O_2$ with cF-***L****-ON1 with formation of the acyclic product **s12**.

By using MALDI-TOF mass spectrometry we experimentally confirmed that it is indeed the case (Figure S5). In particular, irradiation of a mixture of cF-***L****-ON1 (30 μM) and ON2-P as a photosensitizer (1 eq, *m/z* 4193 Da) in aqueous buffered solution (buffer: $(NEt_3H)OAc$, 1 mM, pH 7) with red light for 12 minutes leads to the disappearance of the peak at *m/z* 8145 corresponding to cF-***L****-ON1 and the appearance of the new peak at *m/z* 8178 corresponding to product **s12**.

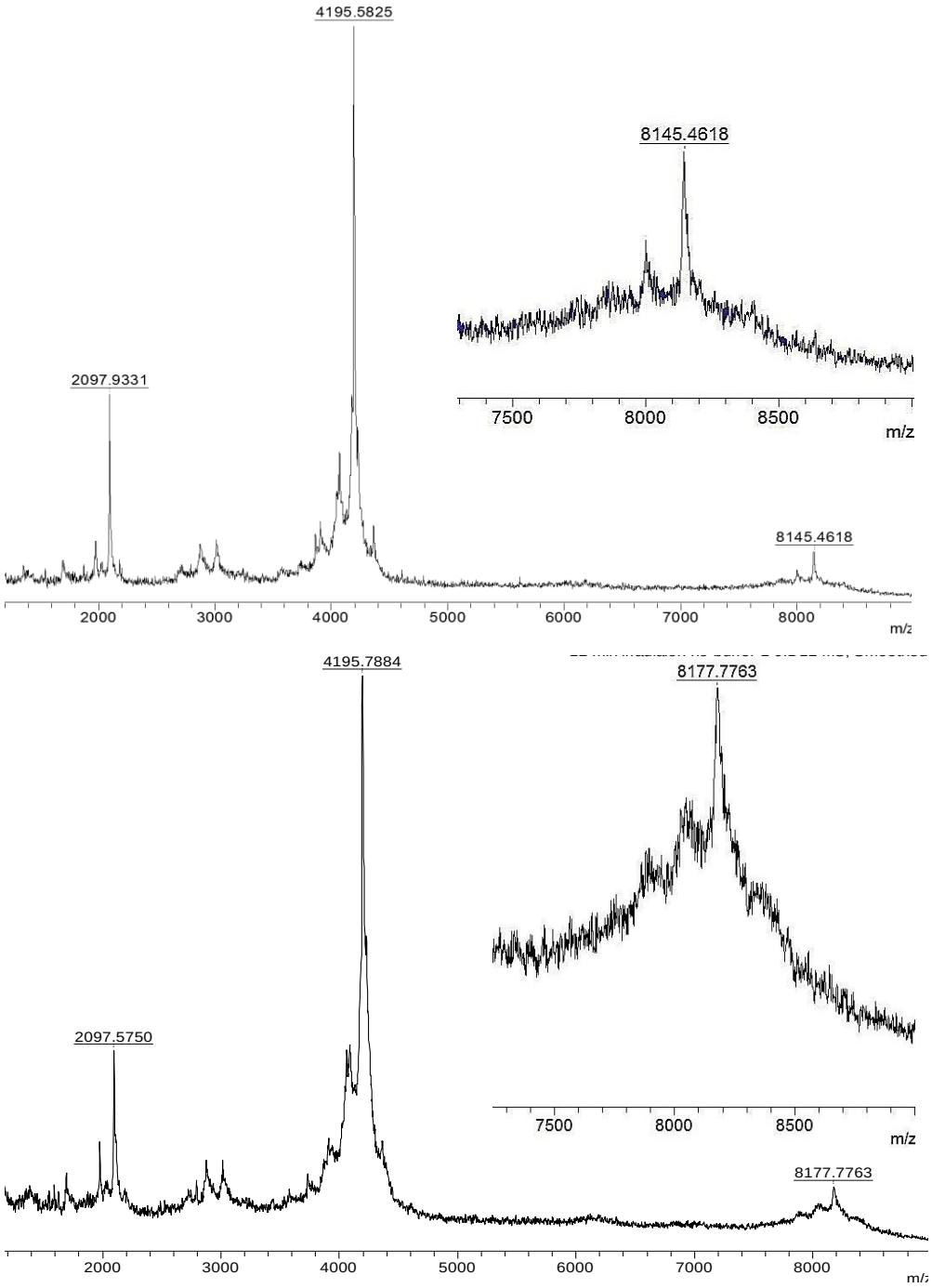

Figure S5. Upper plot: MALDI-TOF spectrum of a mixture of cF-***L*******-ON1 (30 µM) and ON2-P (1 eq) kept for 12 min in the dark; lower plot: the same mixture irradiated for 12 min with red light. In both plots zoomed in spectral regions between m/z 7300 and 8600 were shown. Other experimental conditions are described in the text.

Monitoring nucleic-acid templated fluorogenic reaction trigged with red light

Substrate cF-***L****-ON1 (or cF-***L****-ON1/ON3-Q), a photocatalyst ON2-P (or ON2-P/Q-ON4) and a 42-mer DNA template (NA, a model of β-actin mRNA, Scheme S4)

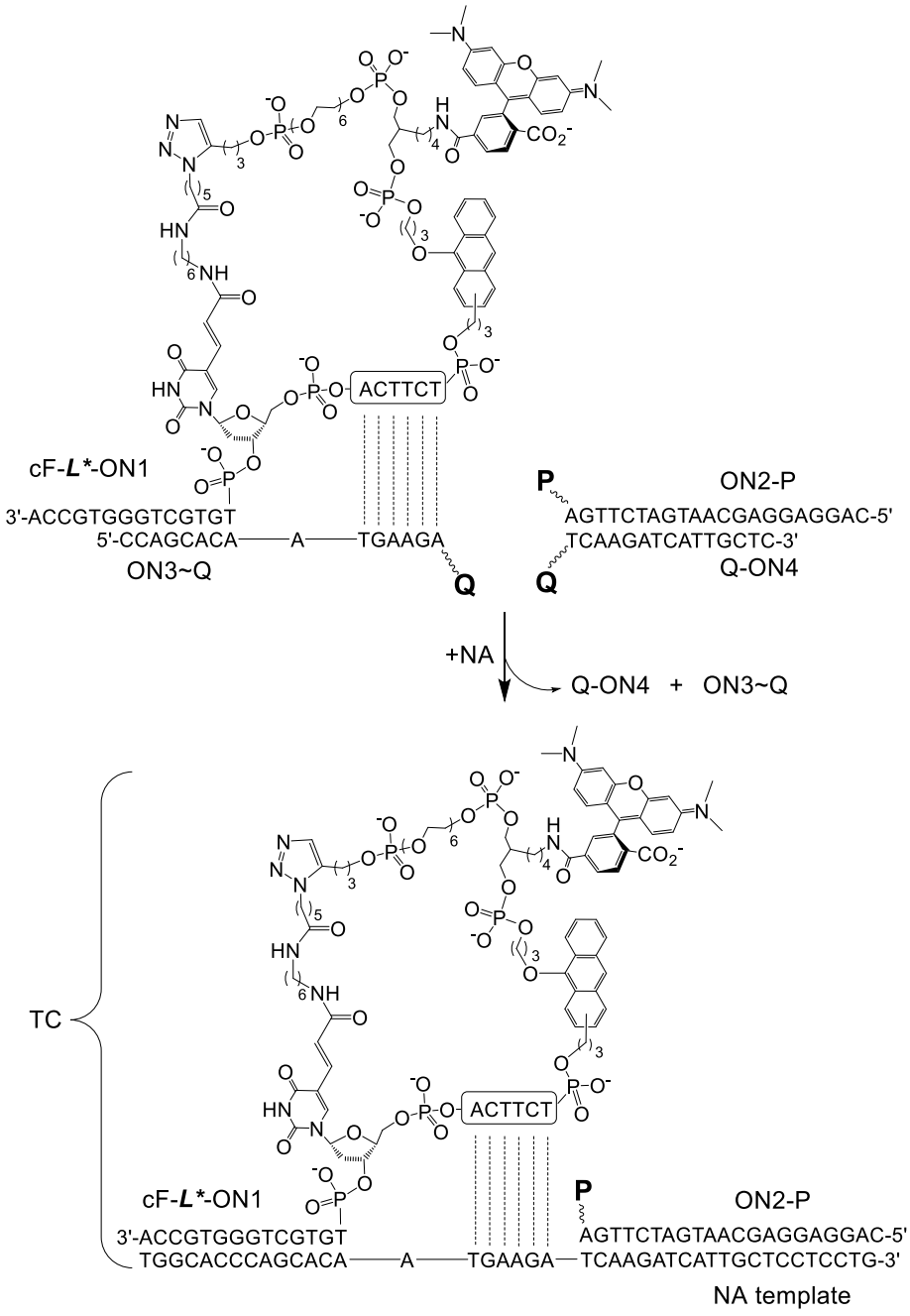

Scheme S4. Outline of the reaction between quenched substrate cF-***L****-ON1/ON3-Q and catalyst ON2-P/Q-ON4 with a nucleic acid template NA leading to formation of a ternary complex TC.

were mixed together in a buffered at pH 7.4 (phosphate buffer, 10 mM) aqueous solution containing NaCl (150 mM) and glutathione (GSH, 5 mM) and allowed to stand for 30 min at 22 °C to achieve hybridization of all strands. Next, these mixtures were irradiated with red light (LED Array 672, λ = 650 nm, 0.29 W) and the increase of the intensity of the fluorescence characteristic for T^{TMR} (λ_{ex}= 550 nm, λ_{em}= 580 nm) was observed. The control mixture lacking the template NA was also included.

Using data shown in Figure 2D, we calculated the initial rate of the template reaction in the mixture of cF-***L****-ON1/ON3-Q (100 nM), catalyst ON2-P/Q-ON4 (1 eq) with a nucleic acid template NA (1 eq) to be 1.8 nM*min^{-1} and that of the background reaction occurring in the absence of the template – 43 pM*min^{-1}.

Evaluation whether the new reaction can be used to detect single mismatches

To enhance the sensitivity of the new reaction in detection of single mismatches within NA's, we replaced catalyst ON2-P/Q-ON4 with its shorter analogue: ON2a-P/Q-ON4a, where ON2a= 3'-AGTTCTAGTAA; ON4a= 5'-TCAAGATCAT. For such shorter oligonucleotides mismatch-induced destabilization of the TC was expected to be higher.

Substrate cF-***L****-ON1/ON3-Q), the short photocatalyst ON2a-P/Q-ON4a and either complementary NA or mismatched NA (where A16→T16 mutation was introduced: 3'-GTCCTCCTCGTTACT*T*GAACTAGAAGTAACACGACCCACGGT) or no NA were mixed together in a buffered at pH 7.4 (phosphate buffer, 10 mM) aqueous solution containing NaCl (150 mM) and glutathione (GSH, 5 mM) and allowed to stand for 30 min at 22 °C to achieve hybridization of all strands. Next, this mixtures were irradiated with red light (LED Array 672, λ = 650 nm, 0.29 W) for 60 min and the intensity of the fluorescence (λ_{ex}= 550 nm, λ_{em}= 580 nm) was detected. The mixture containing matched NA exhibited 1.2-fold higher fluorescence that that of the mixture containing no NA, whereas the fluorescence of the mixture containing matched NA was increased by 3.8-fold. These data confirm that the new reaction is sensitive to single mismatches within NA's.

MD simulations

Extensive molecular dynamics (MD) simulations were used to investigate the duplex formed between the ON1 sequence of cF-***L***-ON1 and the complementary nucleic acid template),

both in a “closed” (Scheme S4) and in an “open” form (Scheme S5). Here, a truncated NA sequence was used (shown in Schemes S4 and S5). Parameter derivation and system set-up were performed following a protocol established previously, therefore only a brief summary is given here.[1] The nucleic acid part of the system was described by the OL15 force field (ff99[2, 3] + bsc0[4] + εζOL1[5] +χOL4[6] +βOL1)[7] and the linkers and dyes by the general amber force field (GAFF)[8, 9] with RESP charges,[10-12] based on calculations (HF/6-31G*//B3LYP/6-31G*)[13-23] with Gaussian 09[24] (optimizations were performed in polarizable continuum model water (PCM,[25-49] see reference [50] for a review)); in agreement with the Amber force fields.[2, 10, 11] Parameters describing interactions at the border between the part described by the nucleic acid force field and the GAFF part were taken from GAFF. The system was solvated in SPC/E water,[51] sodium counterions and additional NaCl were added (total Na^+ concentration: 150 mM, Joung-Cheatham ion parameters).[52] After initial geometry optimization (5,000 steps with restraints (50 kcal mol^{-1} $Å^{-2}$) on DNA/dye/linker, 5000 steps without restraints, switch from steepest descent to conjugate gradients after 500 steps) and 500 ps system heat-up with weak restraints (10 kcal mol^{-1} $Å^{-2}$) on DNA/dye/linker in the NVT ensemble, 1 μs unrestrained NPT Langevin dynamics were performed at 310 K and 1 bar using Amber 16[53] pmemd.cuda on Nvidia Tesla K40m graphics cards. Analyses of the MD data were performed using cpptraj[54] from the Amber[53] suite, and vmd 1.9.3[55, 56] was used for visualization.

For the “closed” simulation (Figure S6), our results show a stable B-DNA nucleic acid structure (mean backbone RMSD, after fitting each frame on the optimized starting structure: 3.46 Å, mean of the phase angle describing the sugar pucker:[57] 148.68 °). Only the first base pair at each terminus of the helix shows some degree of fraying, e.g. with bases like A42 moving away from their ideal Watson-Crick (WC)-bonded position and forming other contacts (e.g. π-π-stacked or “flipped” geometries). The tetramethylrhodamine dye (TAMRA) and the anthracene linker (Ant) are π-π-stacked on each other and on the terminal base pair (T1-A42, especially on T1). A42 is observed in several conformations (WC base-pair with T1, stacked between T1 and G41, near to or stacked with tetramethylrhodamine, “flipped”/exposed to the solvent, stacked with the linker triazole ring, near G41/A40). Plots of

RMSDs, distances, base pairing and sugar puckers that illustrate these observations are provided in Figures S8-S15.

In the “open” simulation (Figure S7), we also observe a stable B-DNA structure (mean backbone RMSD, after fitting each frame on optimized starting structure: 3.49 Å, mean of the phase angle describing the sugar pucker:[57] 148.48 °). Very little fraying occurs (only 1 base pair, A22-T23) at the terminus opposite to the anthracene attachment point. Anthracene (residue 1) is π-π-stacked on the terminal base pair T2-A43 (mainly on T2), while the tetramethylrhodamine/linker moiety is highly mobile, and sometimes shows folded conformations. Tetramethylrhodamine (especially the dimethylamino groups) sometimes forms two different contacts with the DNA backbone in the minor groove, e.g. near the phosphates of C33, G16/G17 and T4, A43. Furthermore, the TAMRA xanthene rings are sometimes close to the triazole ring of the linker. Plots of RMSDs, distances, base pairing and sugar puckers that illustrate these observations are provided in Figures S16-S27.

Simulating larger conformational rearrangements (e.g. DNA hybridization) is currently not feasible with the (unbiased) atomistic simulation approach used here, as the timescale of the MD simulations used (nanoseconds to microseconds) is much shorter than the timescale of DNA hybridization (approx. 15 minutes). Generally, it would be desirable to run much longer (and repeated) simulations, possibly from different initial conformations, and thus achieve much better sampling. However, the intention of the MD simulations shown here was not to simulate the hybridization process, but to show whether the attachment of the dye/linker disturbs the DNA conformation. This was achieved by simulating the “closed” cyclic DNA system as well as the “open” form, with the linker cleaved, in two separate, microsecond-long simulations.

Overall, our MD simulations results confirm that cTMR~L_{CH}~ON1 binds to the NA despite its cyclic structure, and that the duplexes formed are stable and undisturbed by the attachment of the “cyclic” and “open” dye-linker-conjugates.

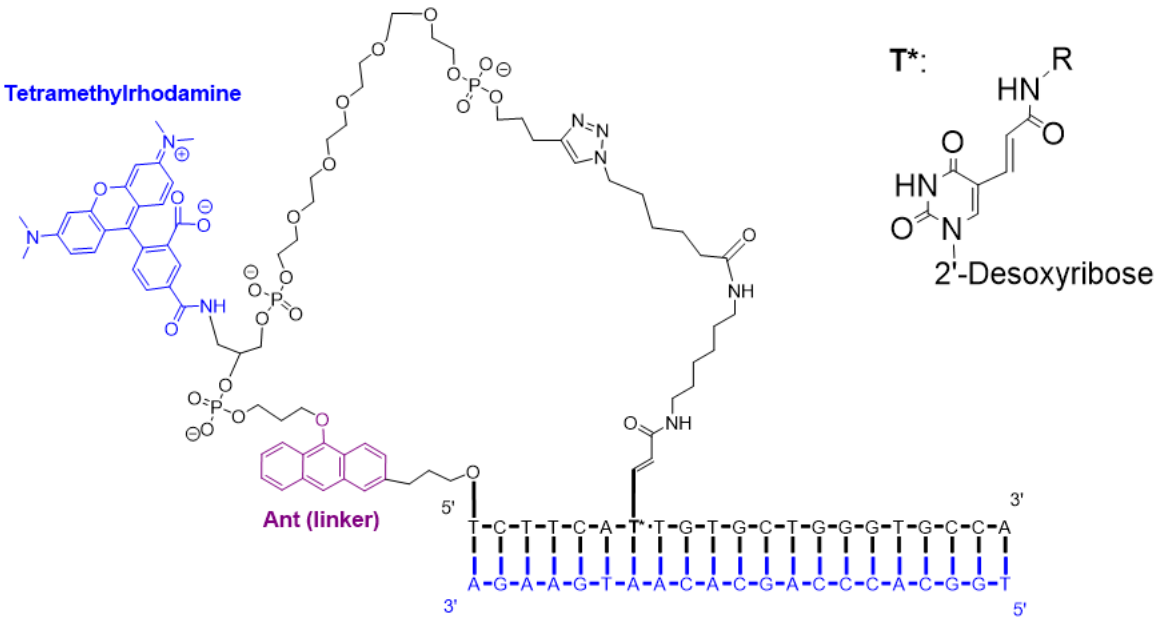

Scheme S5. A structure of substrate cF-***L********-ON1 hybridized with a complementary nucleic acid 3'-AGAAGTAACACGACCCACGGT-5' used for the MD simulations ("closed" system).

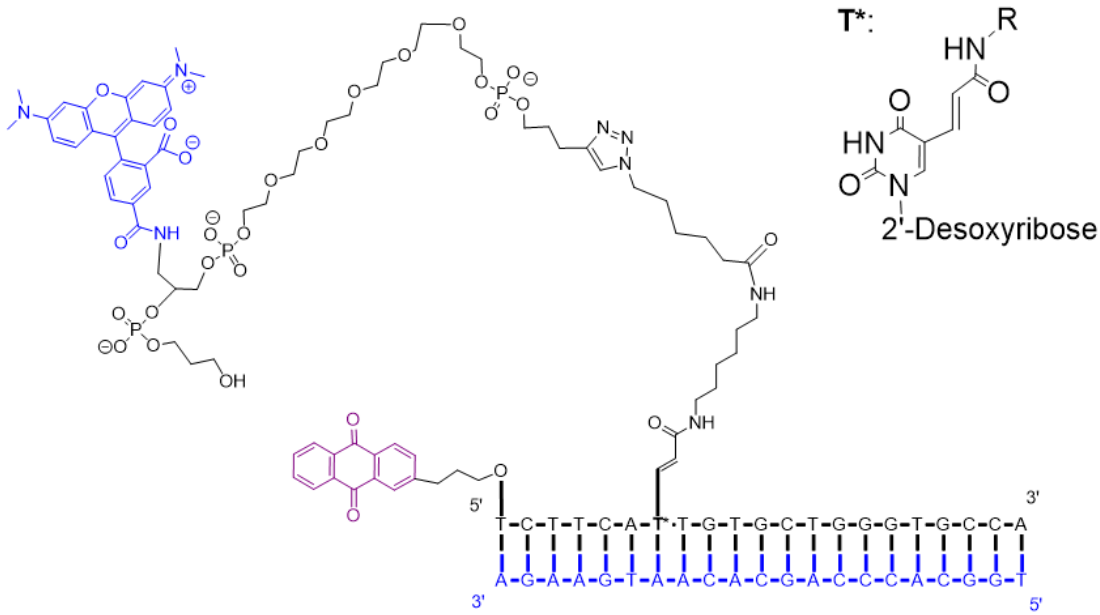

Scheme S6. Cyclic DNA System, "open".

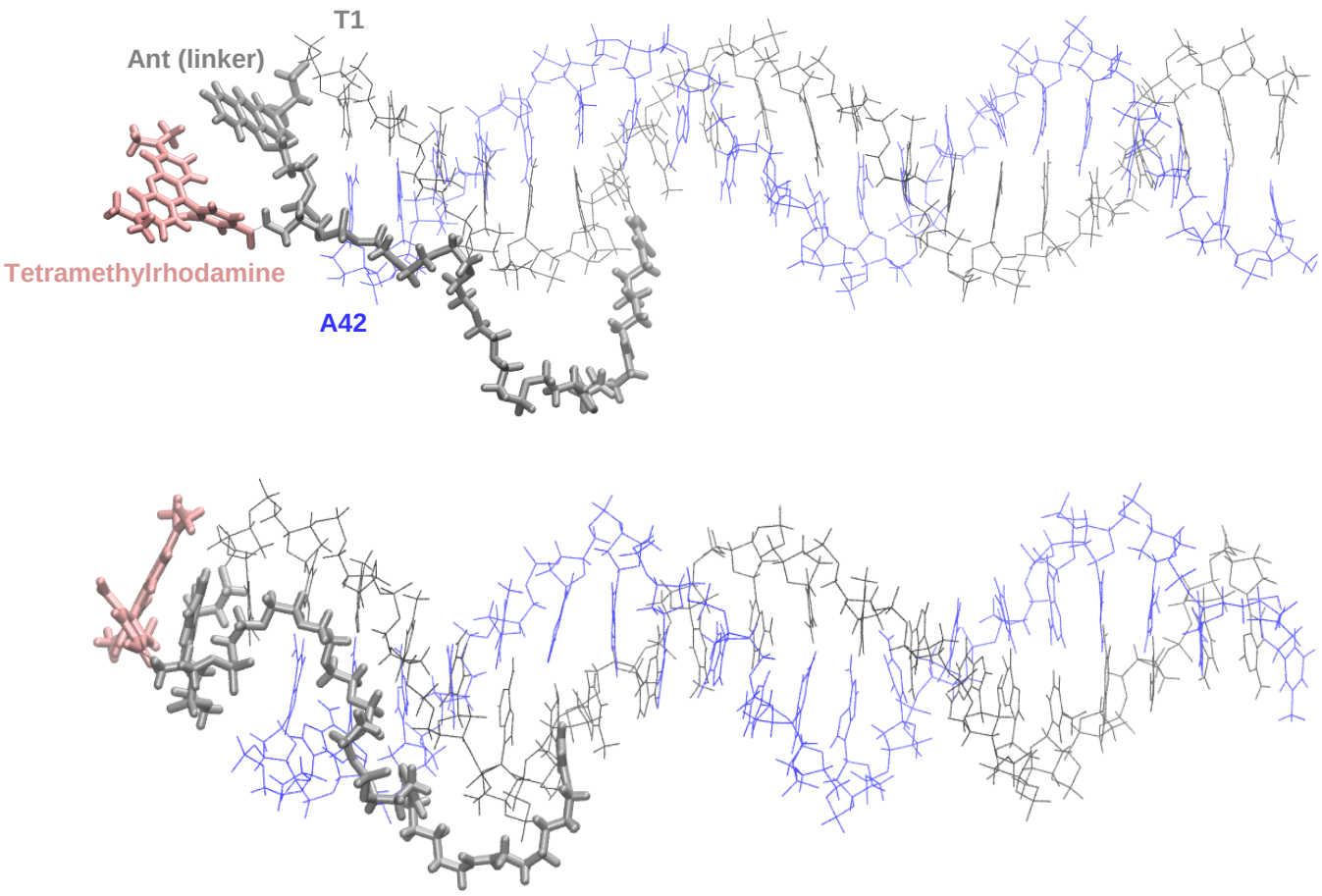

Figure S6. Simulation of the "closed" DNA duplex formed between substrate cF-***L****-ON1 and a complementary DNA strand (its sequence is shown in Scheme S4): Above: structure at 0.6 ns (very close to starting structure), below: snapshot at 1000.5 ns. Colors are as in Scheme 1 in the main text. This figure was created using VMD.[55, 56]

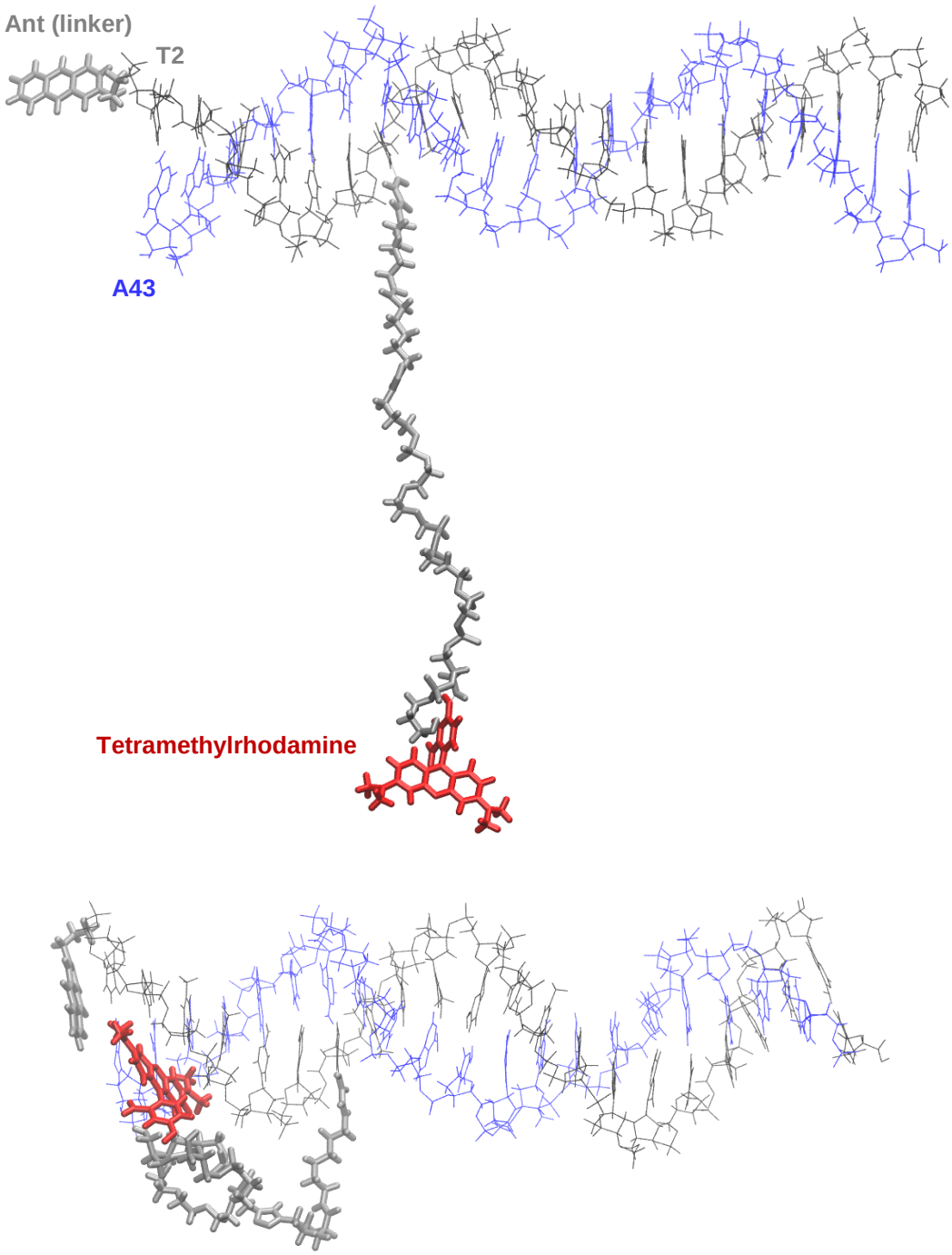

Figure S7. Simulation of cyclic DNA System, open. Above: structure at 0.6 ns (very close to starting structure), below: snapshot at 1000.5 ns. Colors as in Scheme 1 in the main text. Figure created using VMD.[55, 56]

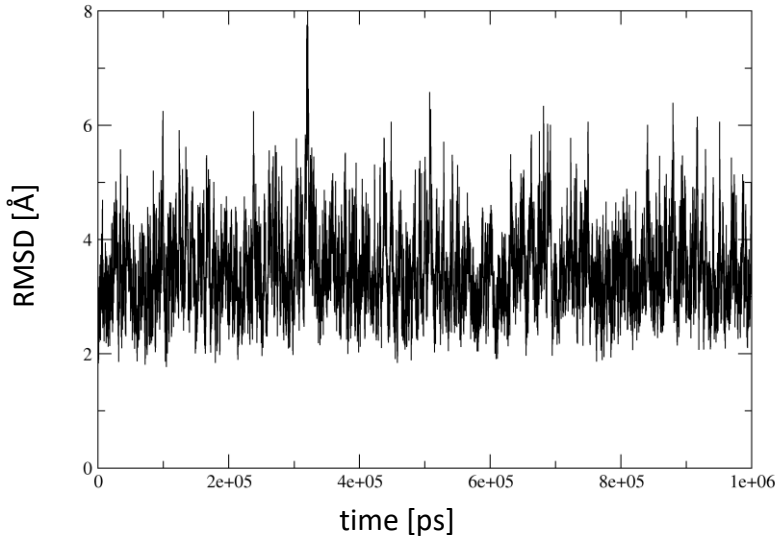

Figure S8. Closed DNA system. RMSD vs. time of DNA backbone atoms, after fitting on the minimized starting structure. Mean: 3.46 Å.

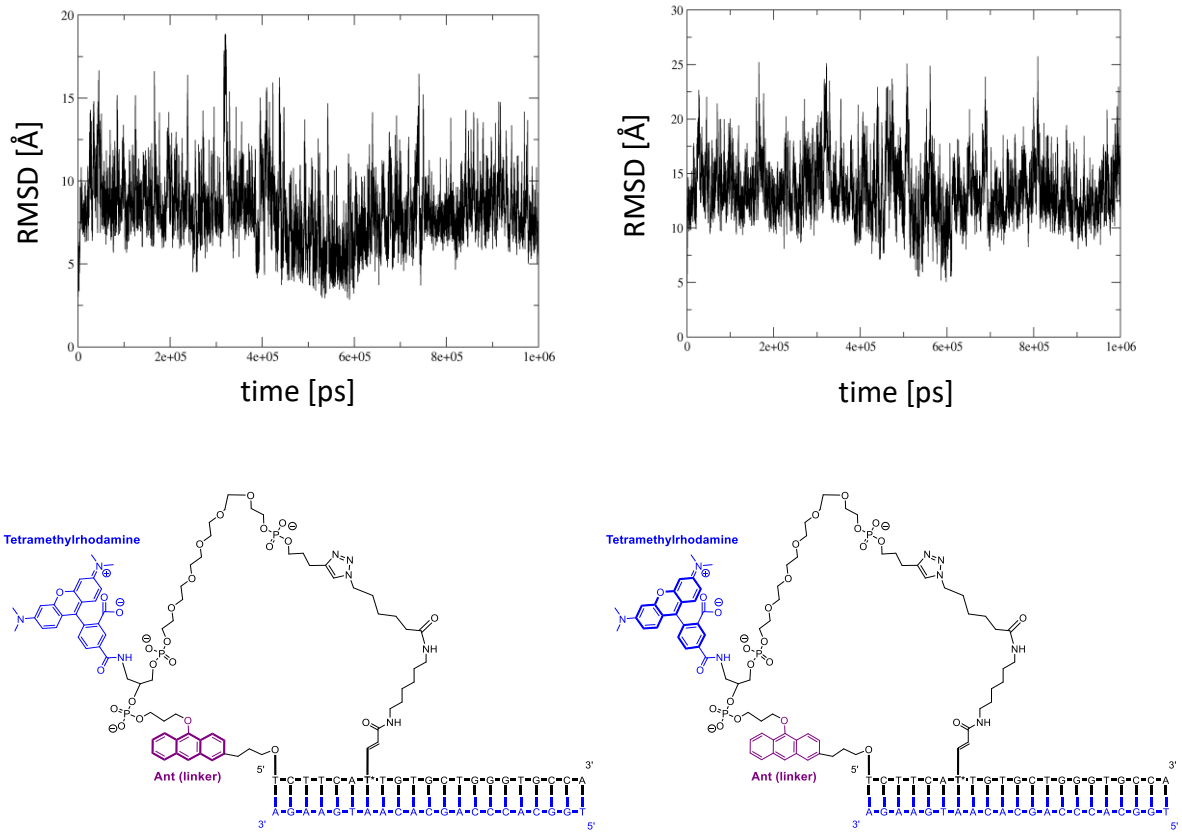

Figure S9. Closed DNA system. RMSD of Ant (left, above) and TAMRA (right, above) ring heavy atoms vs. time, unfitted. Below: Atoms marked in bold were used for RMSD determination.

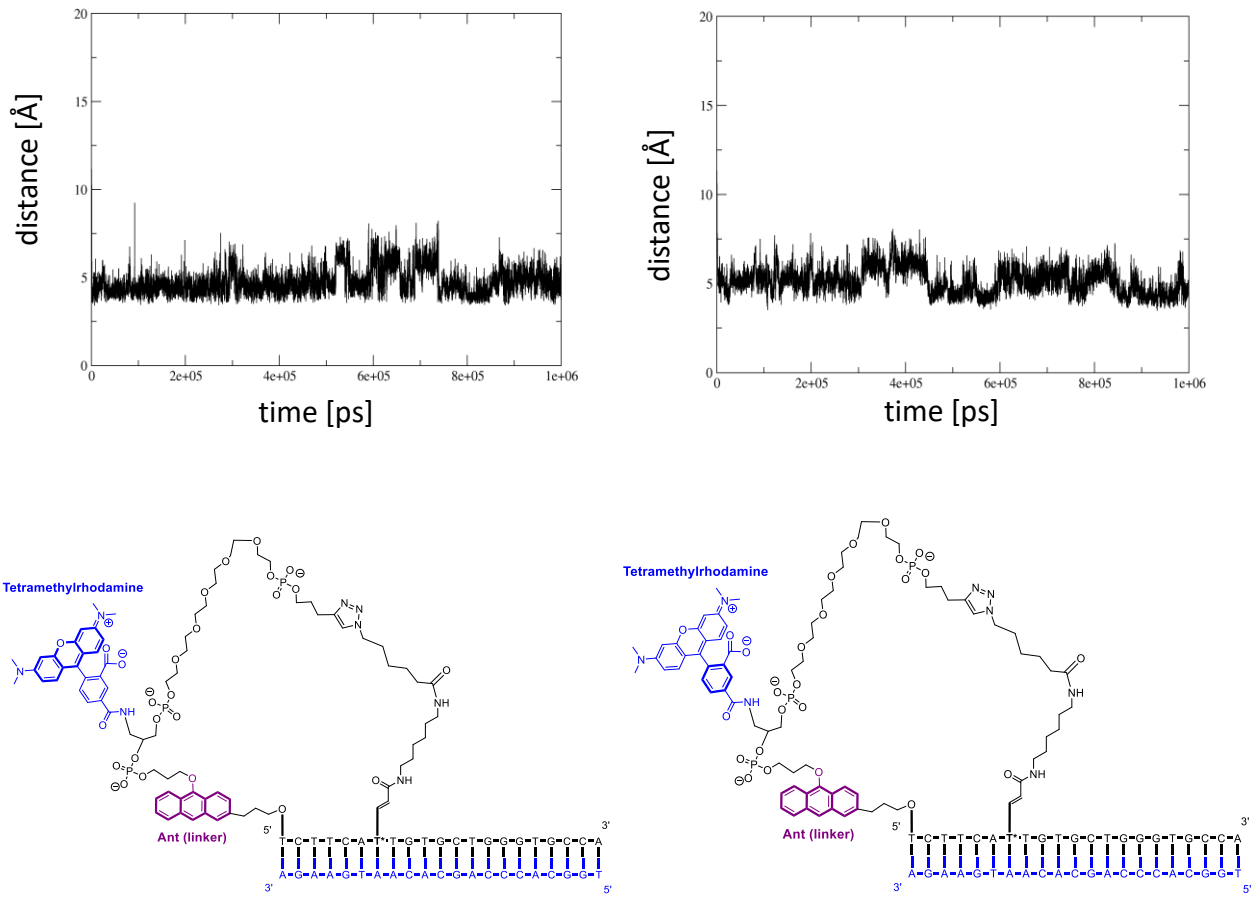

Figure S10. Closed DNA system. Distances between Ant and TAMRA xanthene ring atoms (left, above) and Ant and TAMRA phenyl ring atoms (right, above) vs. time. Below: Atoms marked in bold were used for the measurements.

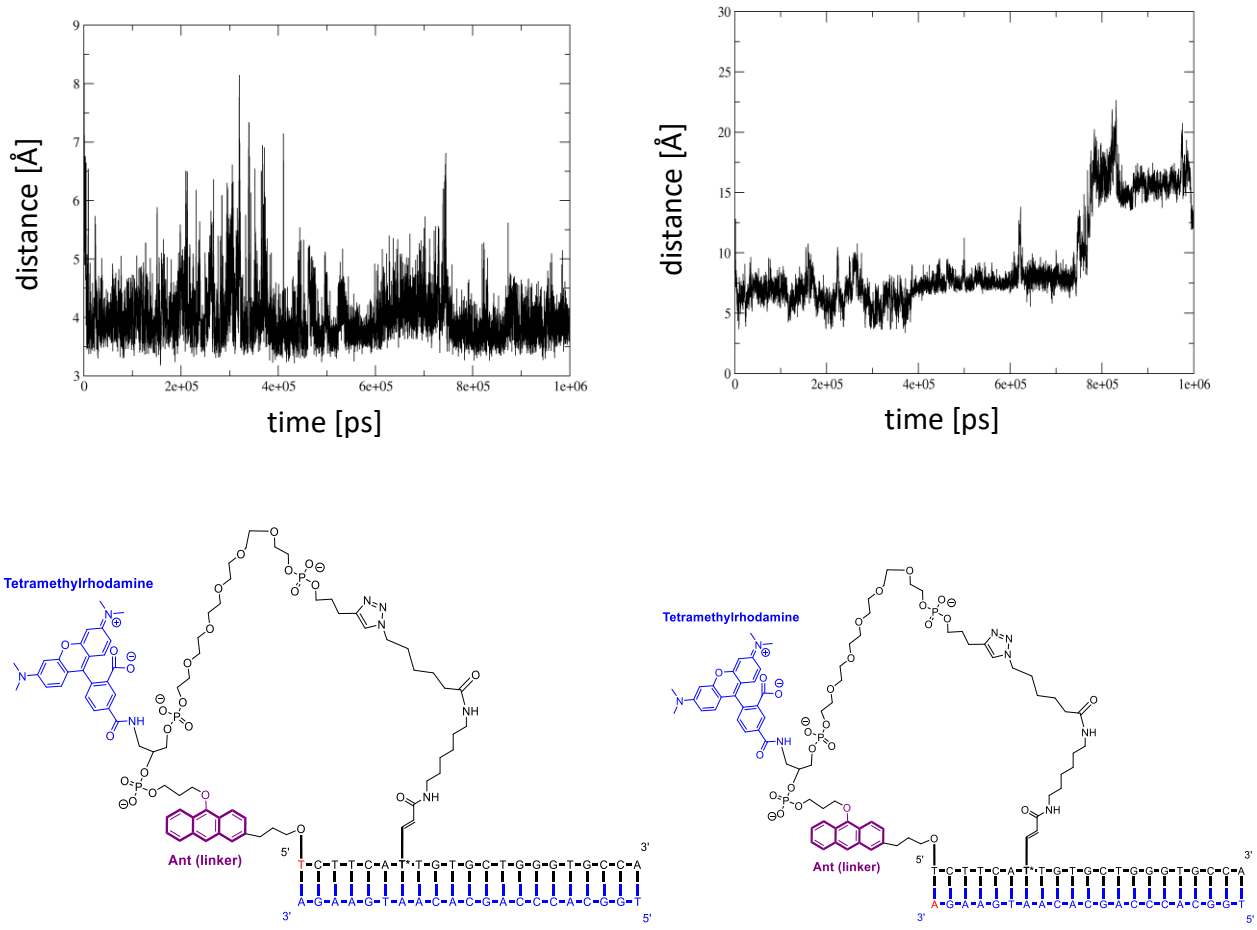

Figure S11. Closed DNA system. Distances between Ant and T1 ring atoms (left, above) and Ant and A42 base ring atoms (right, above) vs. time. Below: Atoms marked in bold or residues marked in red were used for the measurements.

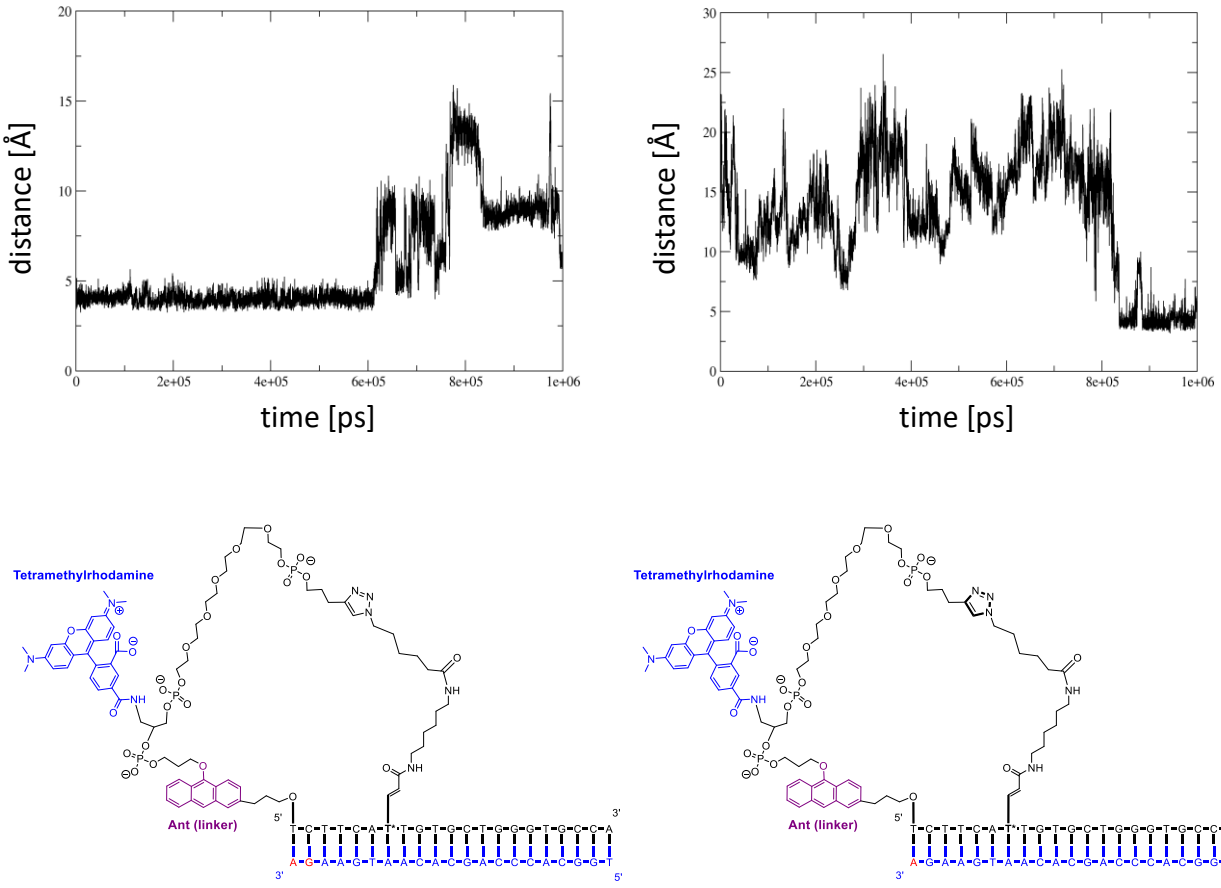

Figure S12. Closed DNA system. Distances between A42 and G41 base ring atoms (left, above) and A42 base ring atoms and linker triazole ring atoms (right, above) vs. time. Below: Atoms marked in bold or residues marked in red were used for the measurements.

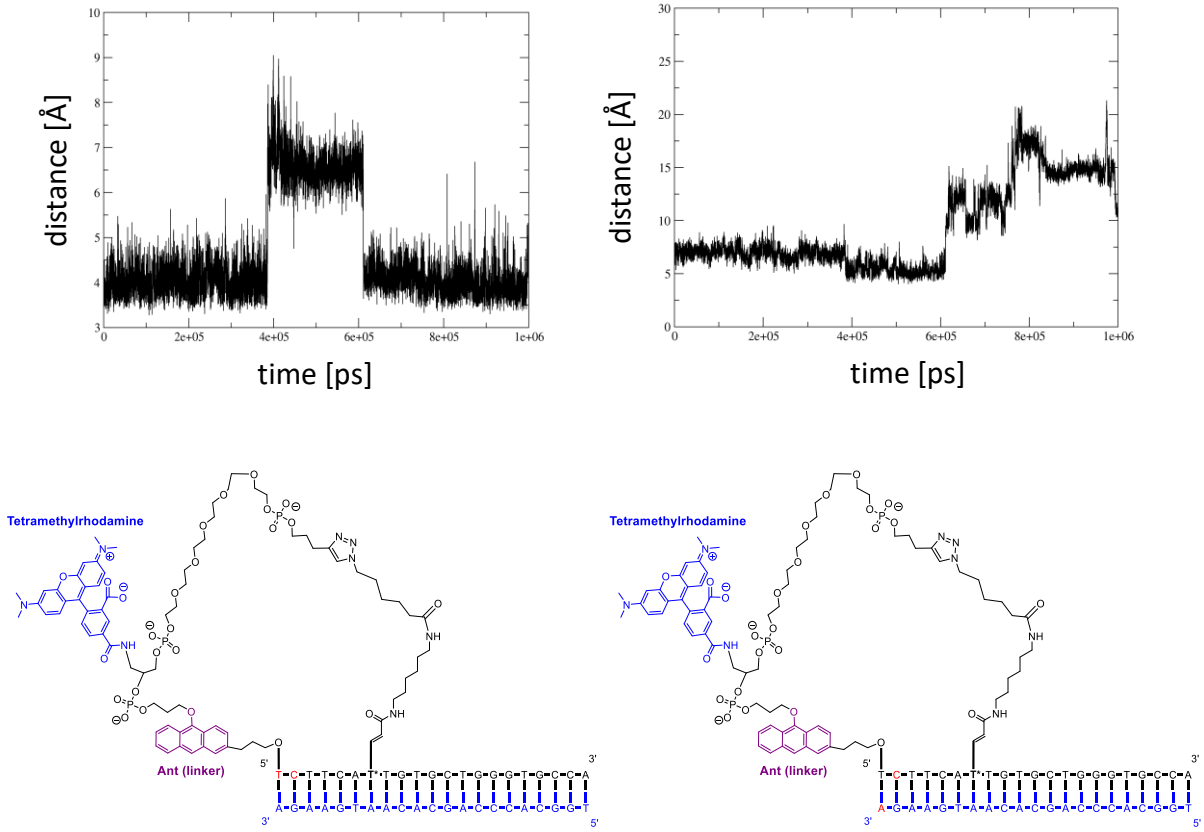

Figure S13. Closed DNA system. Distances between T1 and C2 base ring atoms (left, above) and A42 and C2 base ring atoms (right, above) vs. time. Below: Residues marked in red were used for the measurements.

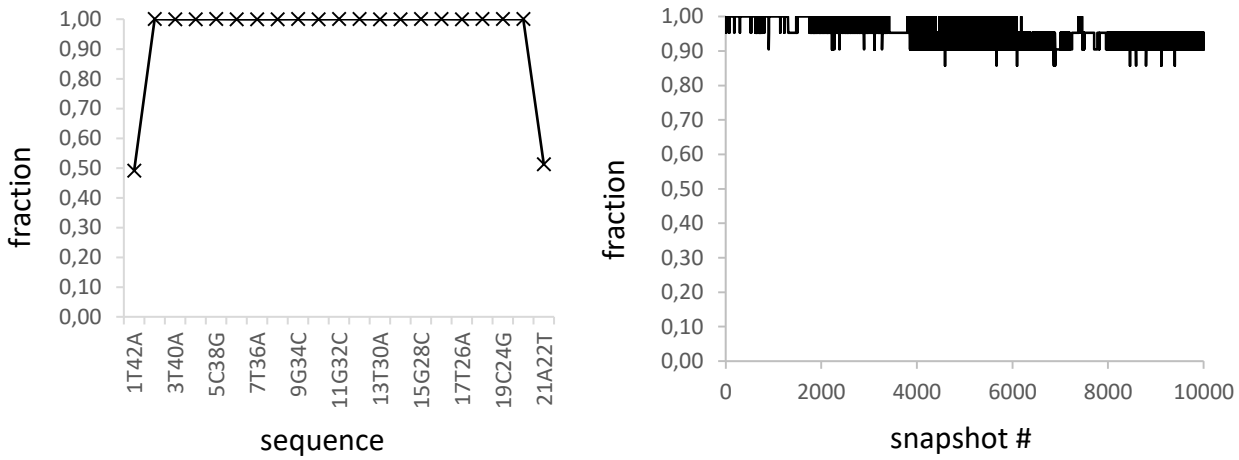

Figure S14. Closed DNA system. Fraction of Watson-Crick base pairs formed vs. sequence (left, averages over 0.5-1000.5 ns) and vs. snapshot number (right).

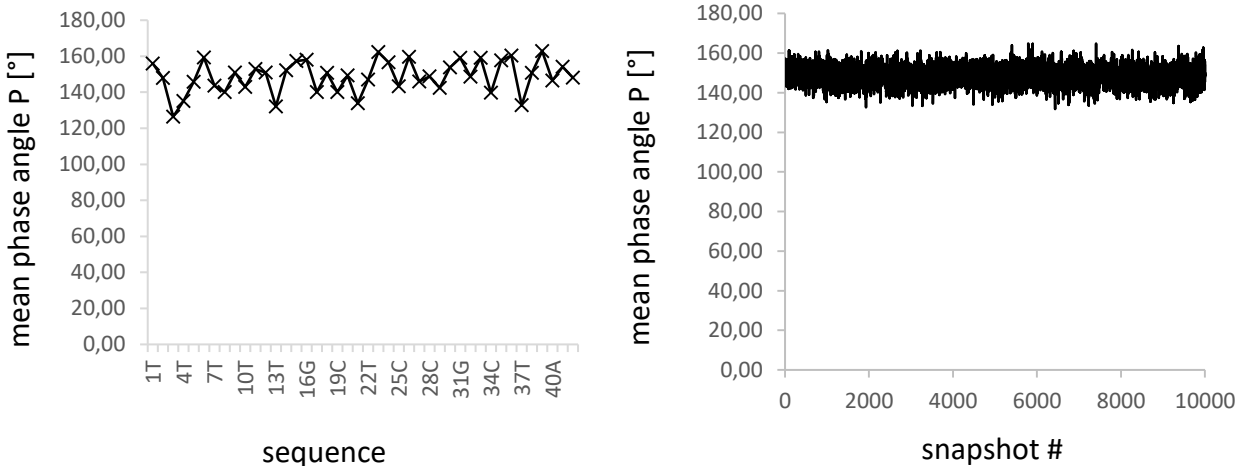

Figure S15. Closed DNA system. Mean value (averages over 0.5-1000.5 ns) of the phase angles describing the sugar pucker of each residue vs. sequence (left) and of all residues versus snapshot number (right, mean: 148.68 °, sugar conformation is C2'-endo/B-DNA).

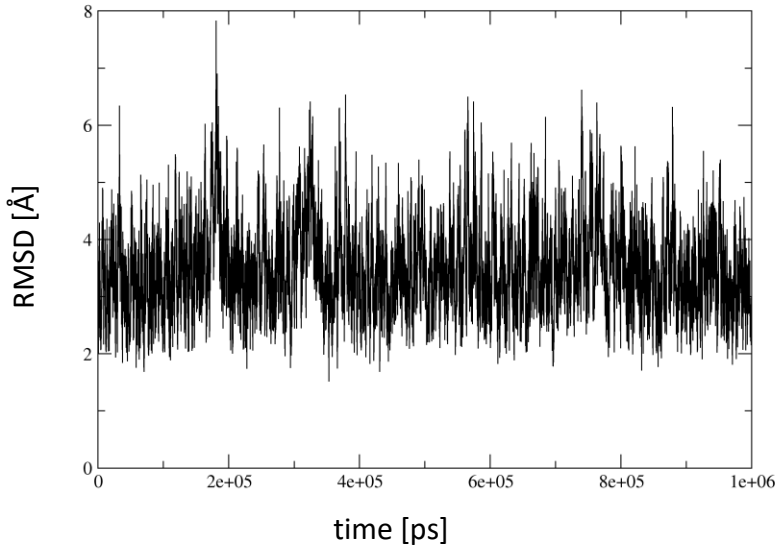

Figure S16. Open DNA system. RMSD vs. time of DNA backbone atoms, after fitting on the minimized starting structure. Mean: 3.49 Å.

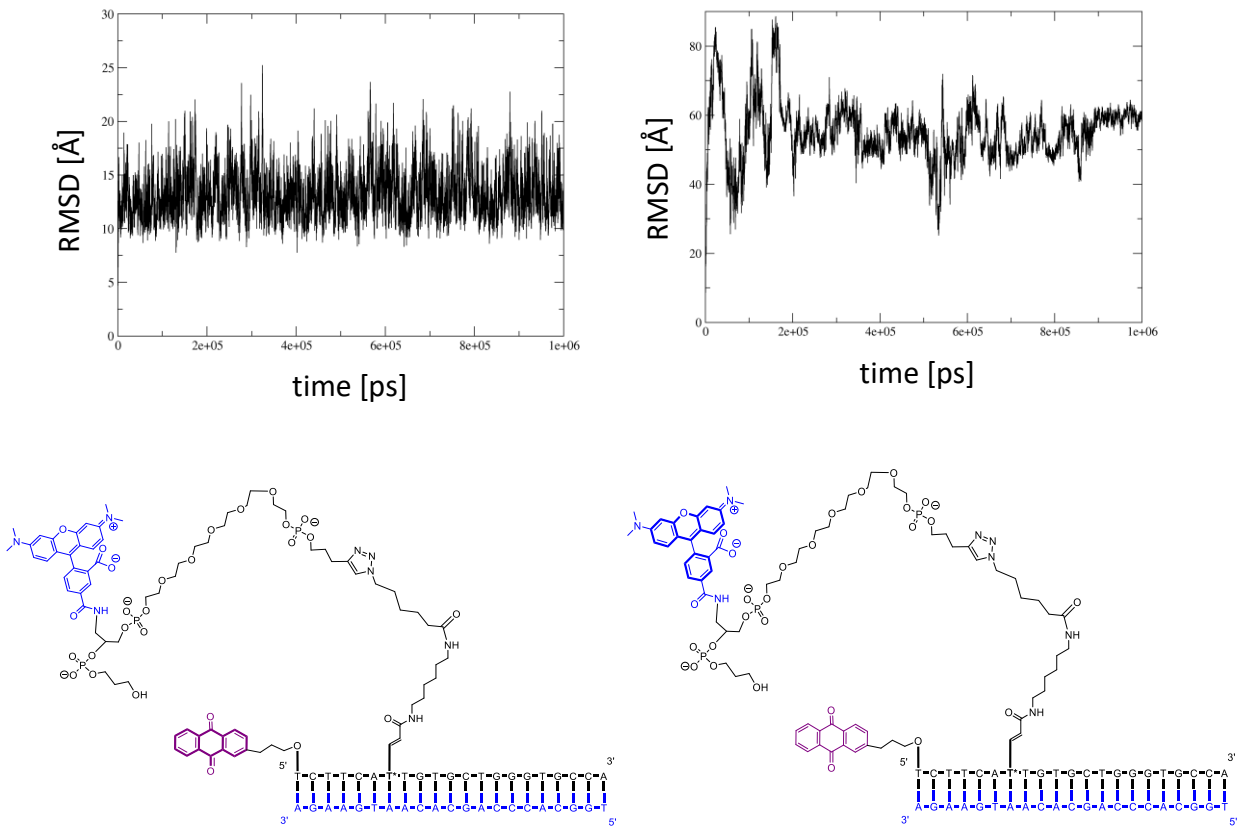

Figure S17. Open DNA system. RMSD of Ant (left, above) and TAMRA (right, above) ring heavy atoms vs. time, unfitted. Below: Atoms marked in bold were used for RMSD determination.

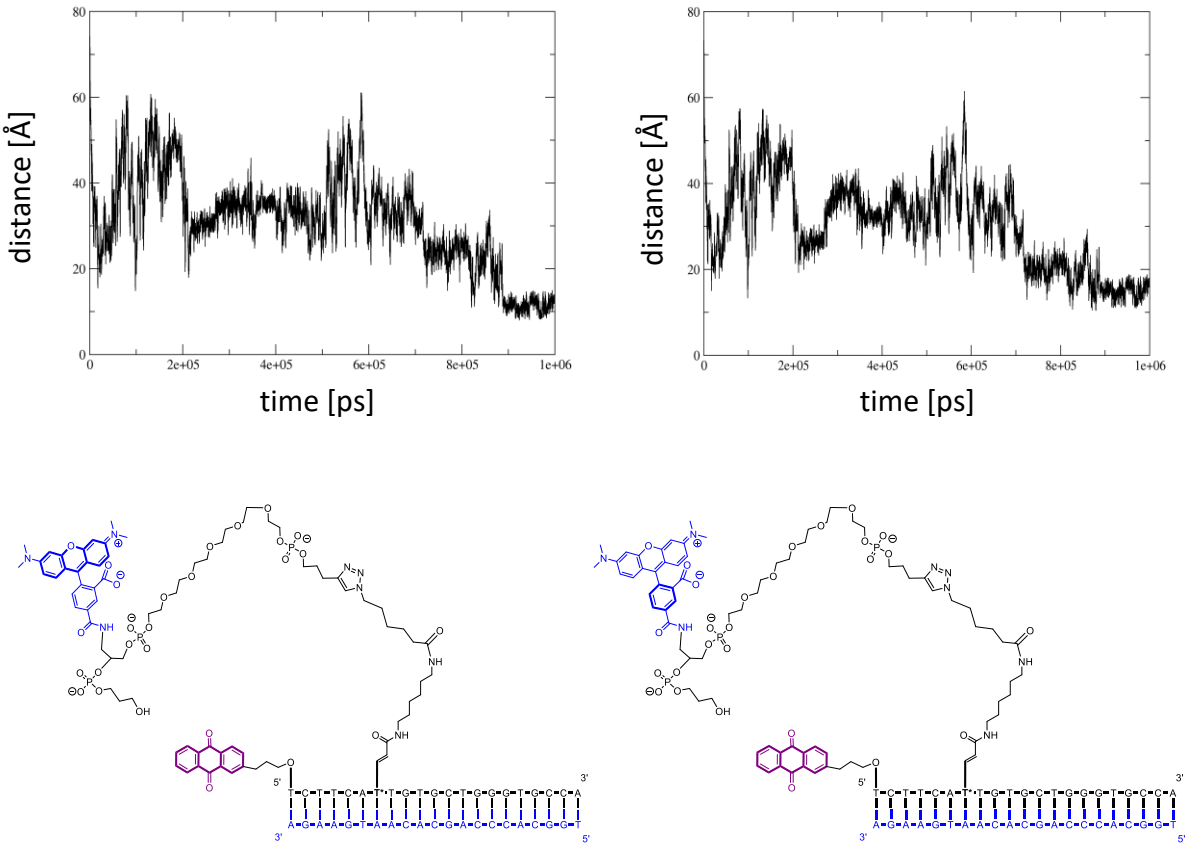

Figure S18. Open DNA system. Distances between Ant and TAMRA xanthene ring atoms (left, above) and Ant and TAMRA phenyl ring atoms (right, above) vs. time. Below: Atoms marked in bold were used for the measurements.

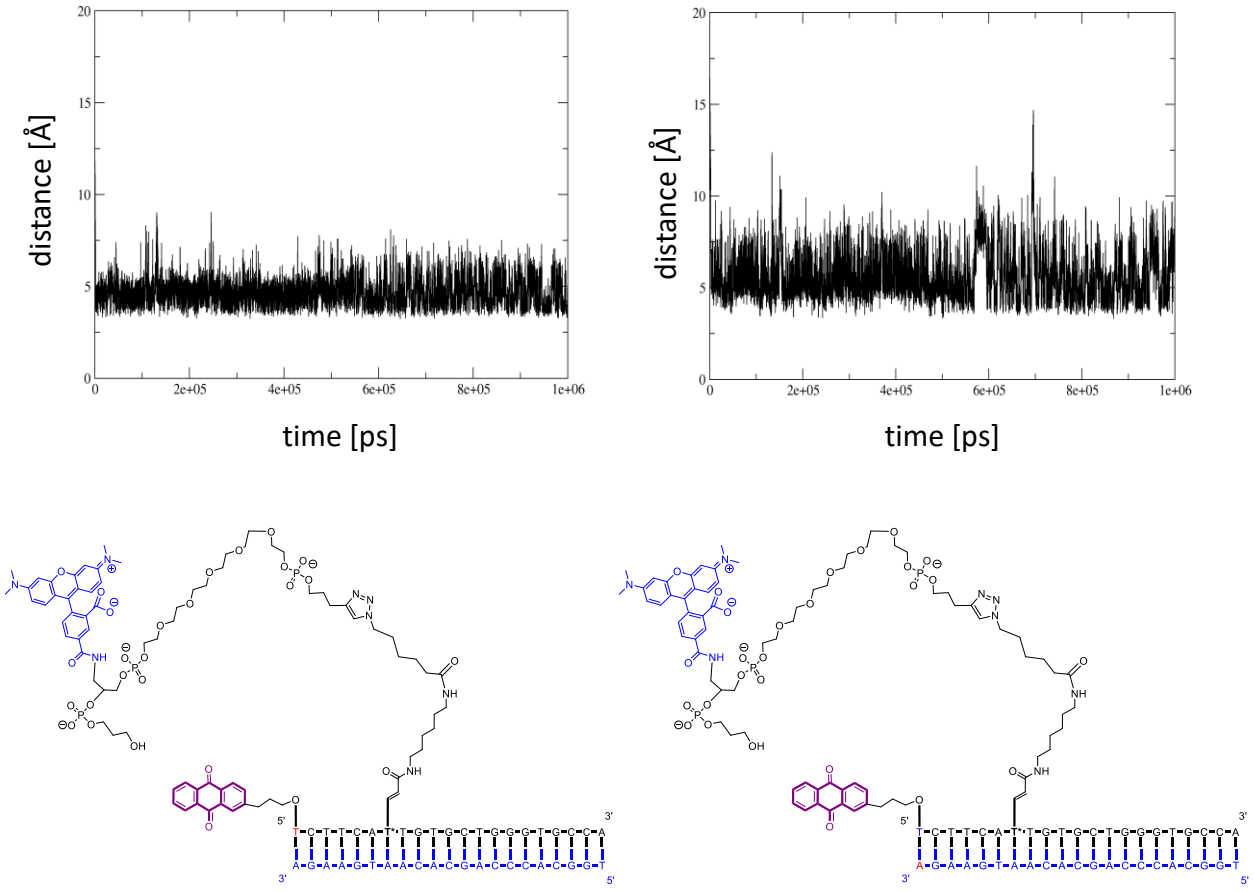

Figure S19. Open DNA system. Distances between Ant ring atoms and T2 base ring atoms (left, above) and Ant ring atoms and A43 base ring atoms (right, above) vs. time. Below: Atoms marked in bold or residues marked in red were used for the measurements.

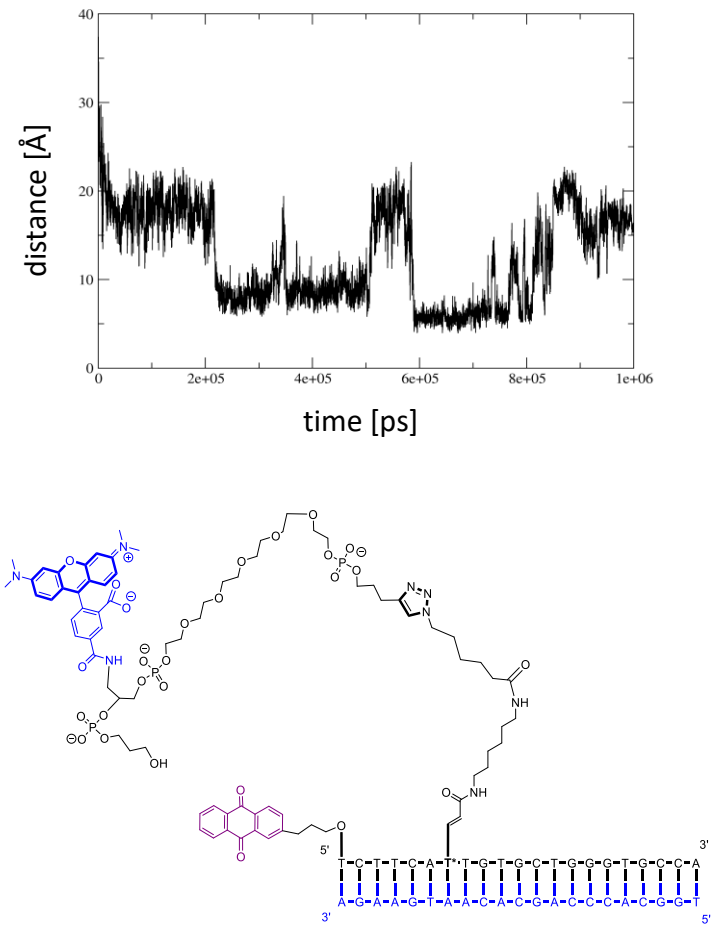

Figure S20. Open DNA system. Distance between TAMRA xanthene and linker triazole ring atoms vs. time (above). Below: Atoms marked in bold were used for the measurements.

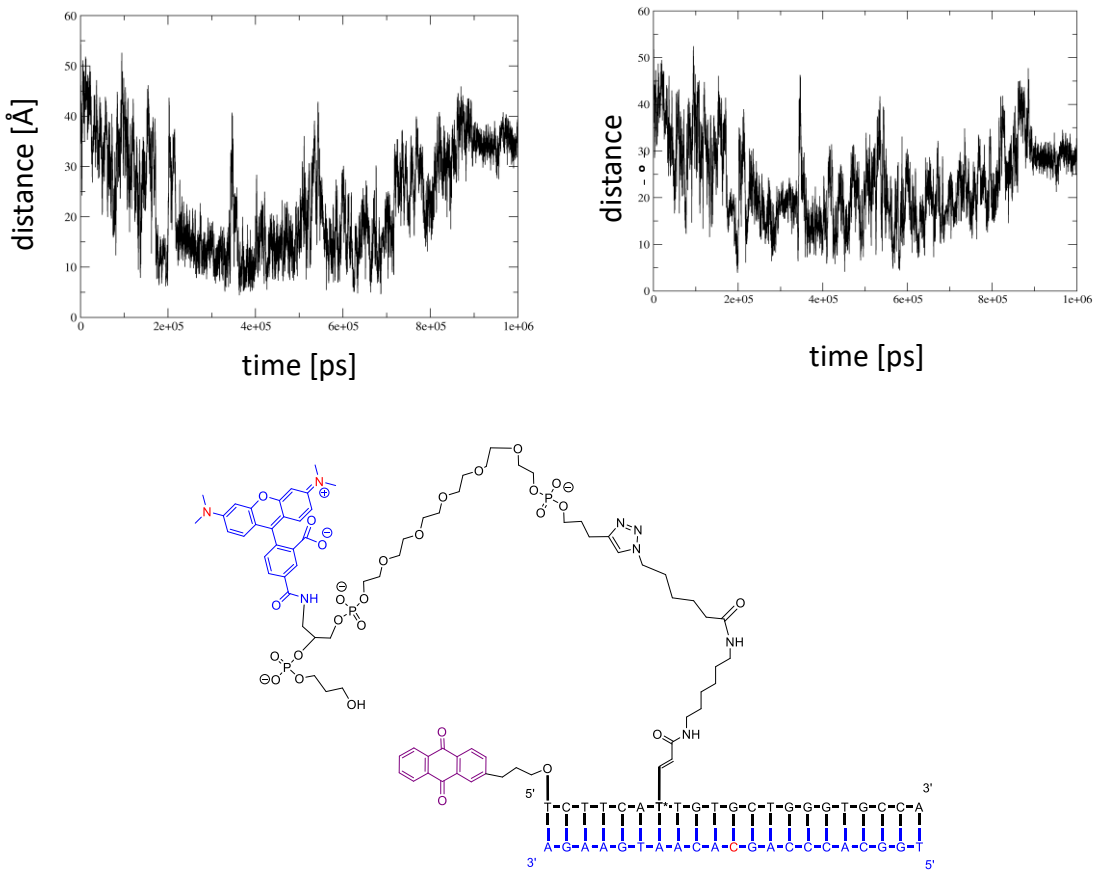

Figure S21. Open DNA system. Distances between TAMRA N9 and C33 OP1 atoms (left, above) and TAMRA N10 and C33 OP1 (right, above) vs. time. Below: Atoms or residues marked in red were used for the measurements.

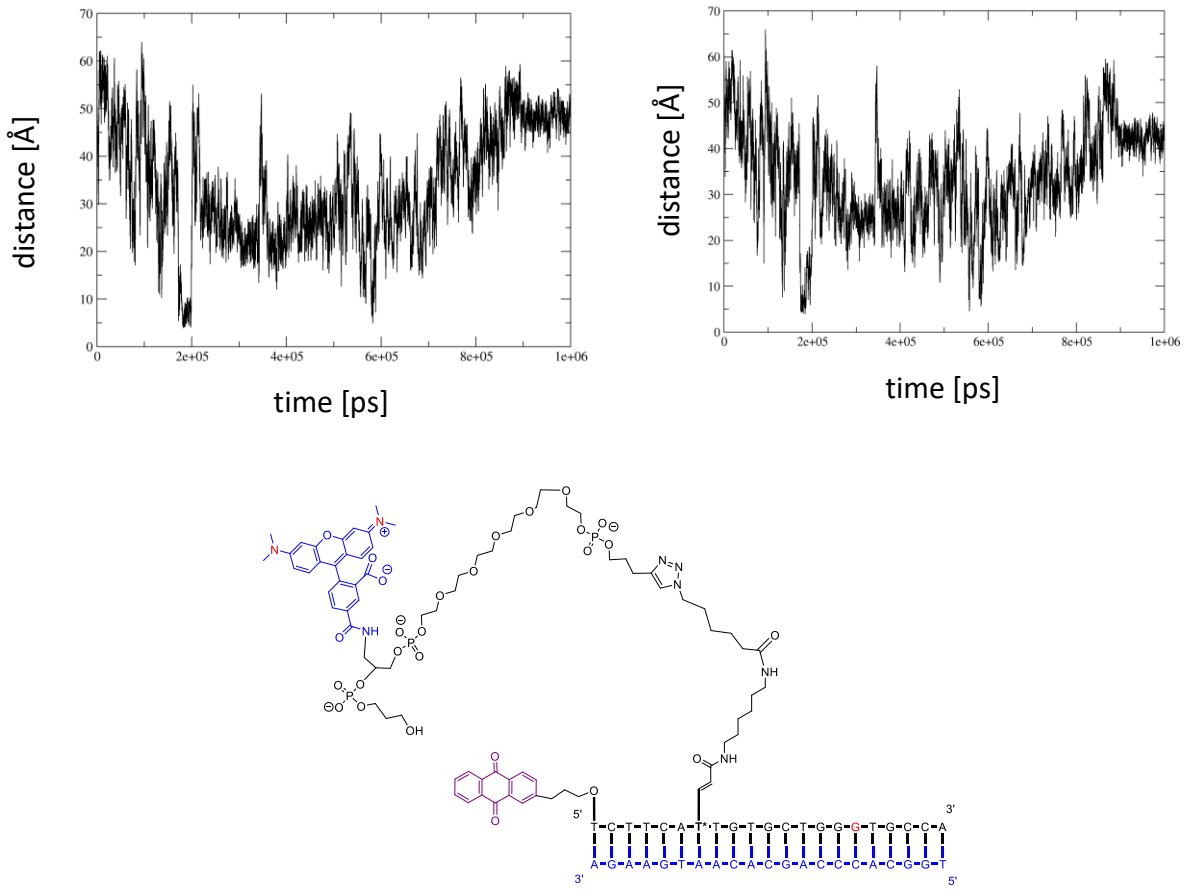

Figure S22. Open DNA system. Distances between TAMRA N9 and G17 OP1 atoms (left, above) and TAMRA N10 and G17 OP1 (right, above) vs. time. Below: Atoms or residues marked in red were used for the measurements.

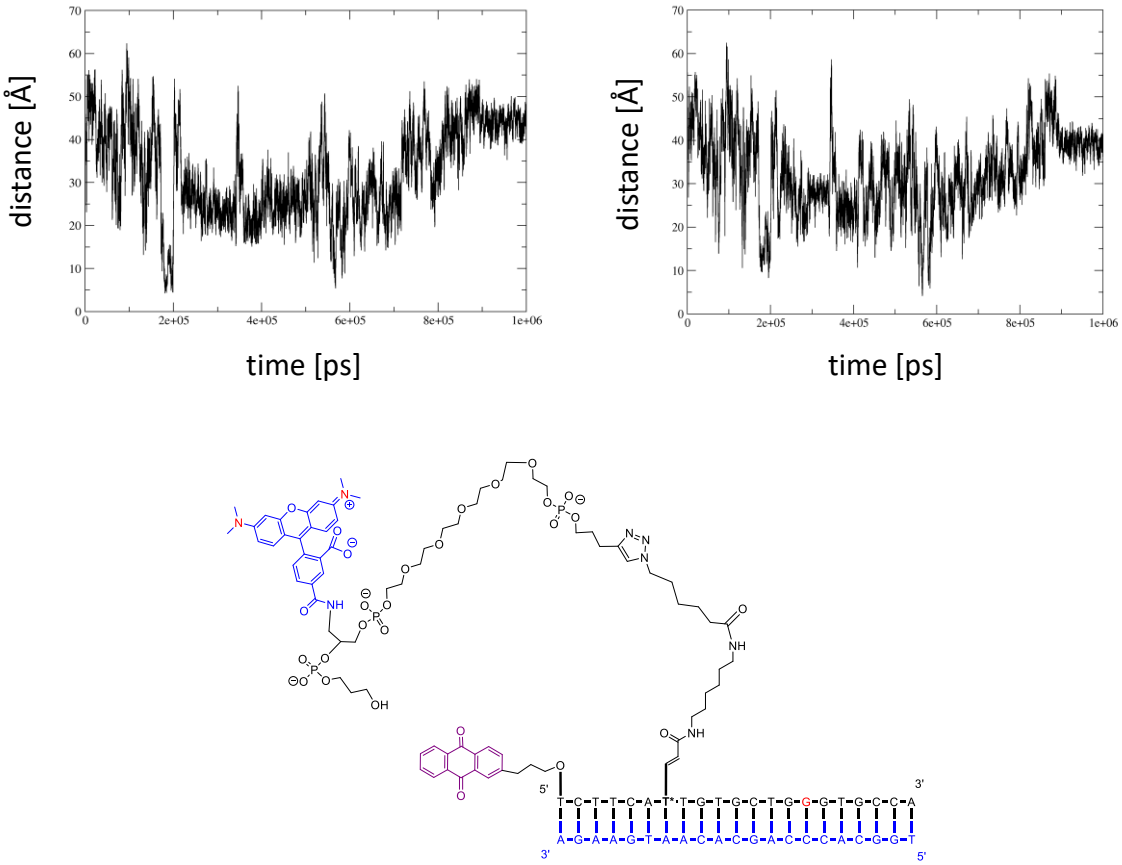

Figure S23. Open DNA system. Distances between TAMRA N9 and G16 OP1 atoms (left, above) and TAMRA N10 and G16 OP1 (right, above) vs. time. Below: Atoms or residues marked in red were used for the measurements.

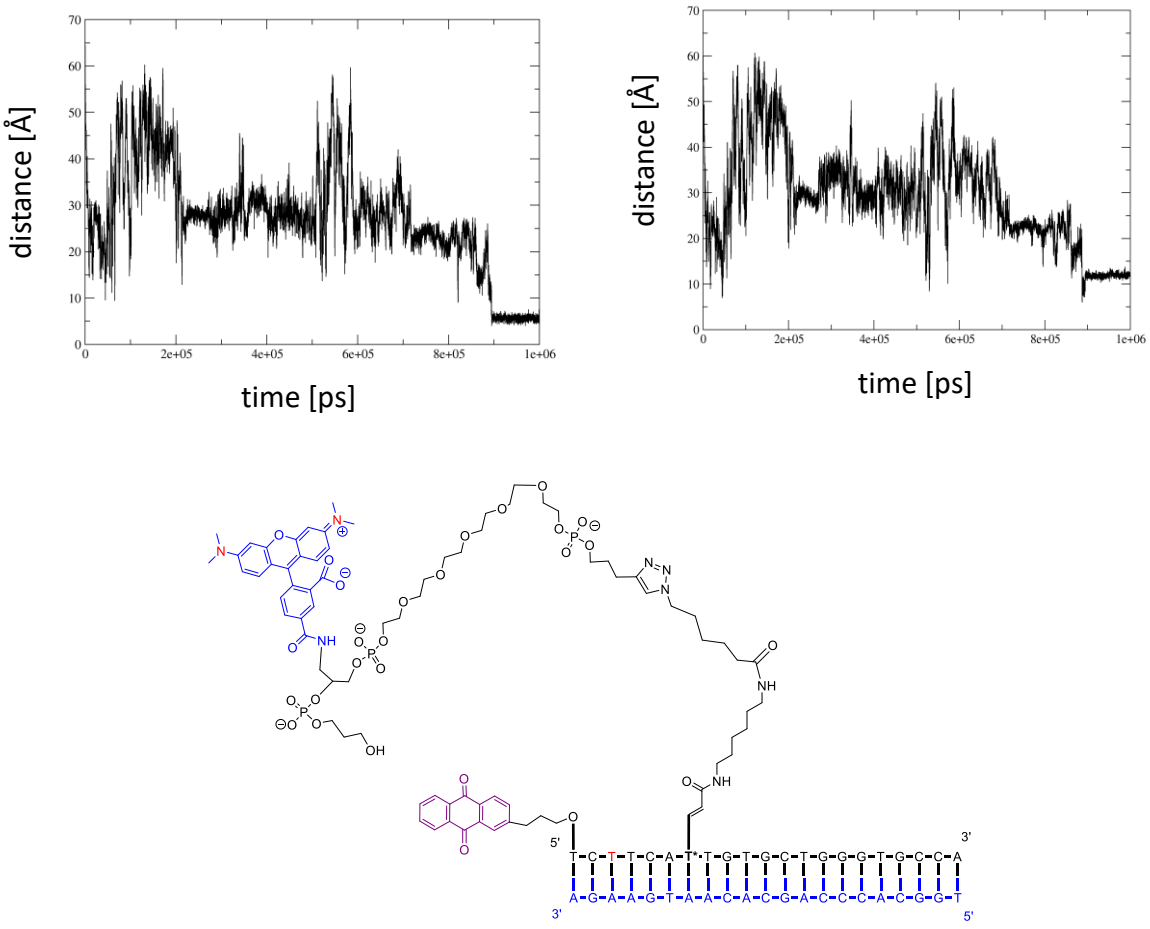

Figure S24. Open DNA system. Distances between TAMRA N9 and T4 OP1 atoms (left, above) and TAMRA N10 and T4 OP1 (right, above) vs. time. Below: Atoms or residues marked in red were used for the measurements.

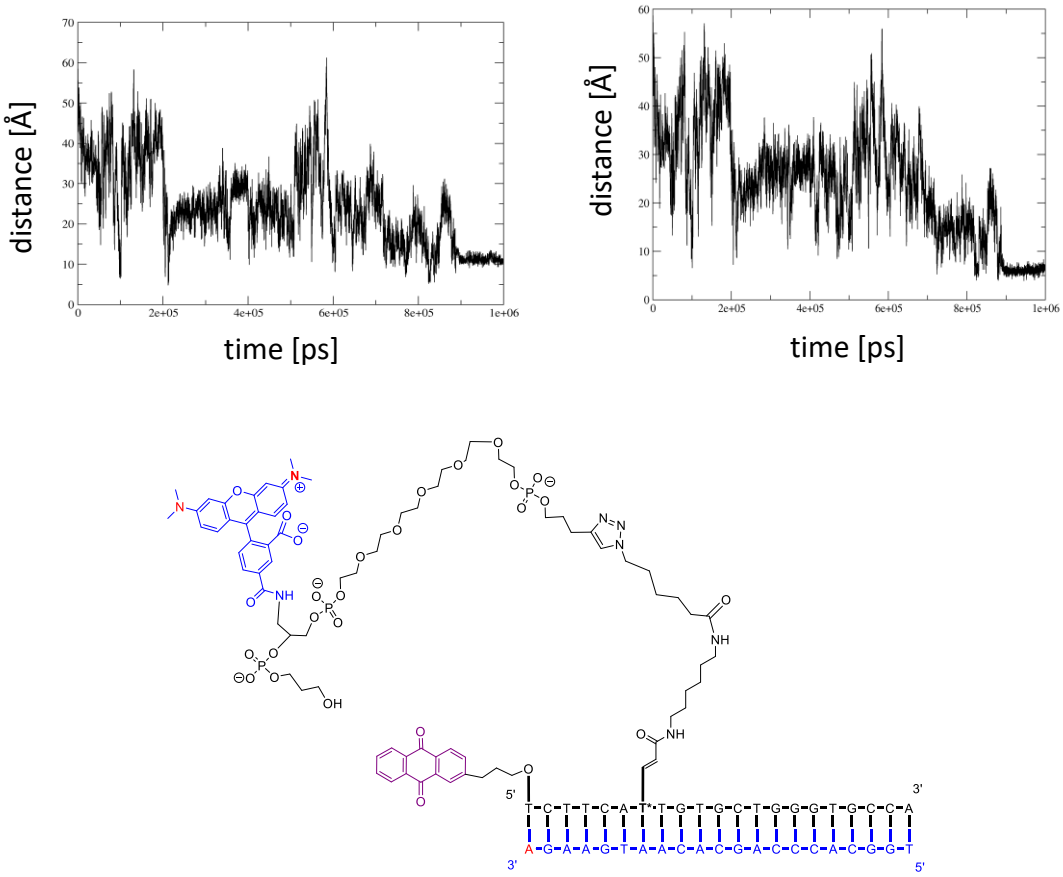

Figure S25. Open DNA system. Distances between TAMRA N9 and A43 OP1 atoms (left, above) and TAMRA N10 and A43 OP1 (right, above) vs. time. Below: Atoms or residues marked in red were used for the measurements.

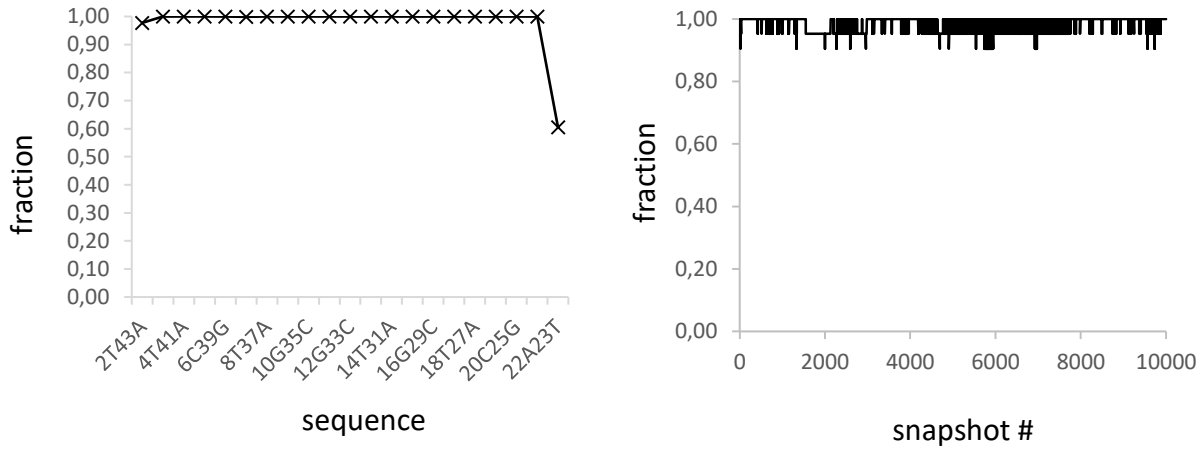

Figure S26. Open DNA system. Fraction of Watson-Crick base pairs formed vs. sequence (left, averages over 0.5-1000.5 ns) and vs. snapshot number (right).

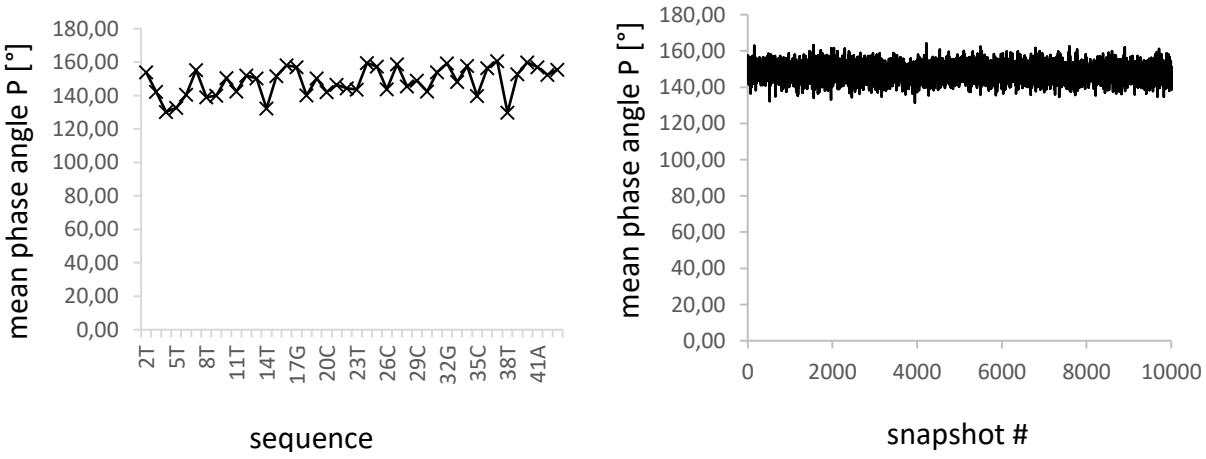

Figure S27. Open DNA system. Mean value (averages over 0.5-1000.5 ns) of the phase angles describing the sugar pucker of each residue vs. sequence (left) and of all residues versus snapshot number (right, mean: 148.48 °, sugar conformation is C2'-endo/B-DNA).

Fluorescence correlation spectroscopy (FCS)

Experiments were performed with a home-built confocal setup. In brief, the excitation light provided by a diode laser (532 nm 50 mW, Obis, Coherent Inc., Santa Clara, USA) was coupled into a single-mode optical fibre (P1-460B-FC-2, Thorlabs, Newton, USA), expanded with a collimator (6 mm, Qioptiq Photonics GmbH, Waltham, USA) and focussed onto the sample using a dichroic mirror (Dualline zt532/642rpc, AHF Analysentechnik AG, Tübingen, Germany) and a water immersion objective (UPLSAPO, 60x, NA 1.20, Olympus Deutschland GmbH, Hamburg, Germany). The emitted light passed a pinhole (Diameter: 100 µm, Thorlabs, Newton, USA), was filtered by a bandpass filter (ET 570/60) and focused onto an avalanche photodiode (APD) (SPCM-AQRH-14, PerkinElmer Optoelectronics, Waltham, USA). The fluorescence signal was processed with a correlator card (Flex03lq, correlator.com, Zhejianj, China).

Sample preparation for FCS experiments

100 nM biotinylated NA template, 200 nM substrate cF-***L***-ON1 and optional 200 nM ON2~P were hybridized in a mixture of 50 µl 1× TAE with 12.5 mM $MgCl_2$ generating the used dsDNA. The strands were annealed by using a temperature gradient starting with incubation for 5 min at 85°C and then cooling down to 20°C with -0.1°C/s. 75 µL of 1 nM hybridized dsDNA in PBST (1x PBS + 0.05% Tween-20) were placed onto a Menzel microscope slide with a single depression (VWR) and covered with a coverslide (no. 1.5, 25 × 50 mm, VWR). FCS measurements were performed with following parameters: acquisition time = 300 s, laser power = 74 µW (measured in front of the objective), temperature 25°C, and a constant imaging depth of 100 µm. The sample was irradiated with a red LED (λ_{max} = 634 nm, emitted power = 15.5 mW; Osram, Munich, Germany). Each experiment was repeated 3 times.

The FCS autocorrelation functions were approximated by a two-dimensional diffusion model for a single species with an additional term accounting for photophysical processes as described in Gatterdam et al.[58]

$$G(\tau) = \frac{1}{N}(1+\frac{\tau}{\tau_D})^{-1}\left(1+\frac{T}{1-T}\right)\exp(-\frac{\tau}{\tau_D})$$

Table S1. Fit parameter of FCS measurements.

Sample	hν	number of particles	Diffusion-time (τ_D) [s]	Intensity [kHz]	Brightness /particle	Triplet fraction	Triplet-Lifetime (τ_T) [s]
NA + cF-***L****-ON1	-	6.84	$1.08 \cdot 10^{-3}$	34733.69	5074.71	0.22	$7.00 \cdot 10^{-5}$
	+	7.66	$1.03 \cdot 10^{-3}$	44812.58	5846.72	0.25	$7.00 \cdot 10^{-5}$
NA + cF-***L****-ON1 + ON_2~P	-	5.72	$1.15 \cdot 10^{-3}$	20124.34	3517.71	0.20	$7.00 \cdot 10^{-5}$
	+	7.57	$0.93 \cdot 10^{-3}$	41852.64	5527.09	0.24	$7.00 \cdot 10^{-5}$

References

1. F. R. Beierlein, M. Paradas Palomo, D. I. Sharapa, O. Zozulia, A. Mokhir and T. Clark, *PLoS ONE*, 2016, **11**, e0160229.
2. W. D. Cornell, P. Cieplak, C. I. Bayly, I. R. Gould, K. M. Merz Jr., D. M. Ferguson, D. C. Spellmeyer, T. Fox, J. W. Caldwell and P. A. Kollman, *J. Am. Chem. Soc.*, 1995, **117**, 5179-5197.
3. J. Wang, P. Cieplak and P. A. Kollman, *J. Comput. Chem.*, 2000, **21**, 1049-1074.
4. A. Pérez, I. Marchán, D. Svozil, J. Sponer, T. E. Cheatham III, C. A. Laughton and M. Orozco, *Biophys. J.*, 2007, **92**, 3817-3829.
5. M. Zgarbová, F. J. Luque, J. Šponer, T. E. Cheatham, M. Otyepka and P. Jurečka, *J. Chem. Theory Comput.*, 2013, **9**, 2339-2354.
6. M. Krepl, M. Zgarbová, P. Stadlbauer, M. Otyepka, P. Banáš, J. Koča, T. E. Cheatham, P. Jurečka and J. Šponer, *J. Chem. Theory Comput.*, 2012, **8**, 2506-2520.
7. M. Zgarbová, J. Šponer, M. Otyepka, T. E. Cheatham, R. Galindo-Murillo and P. Jurečka, *J. Chem. Theory Comput.*, 2015, **11**, 5723-5736.
8. J. Wang, R. M. Wolf, J. W. Caldwell, P. A. Kollman and D. A. Case, *J. Comput. Chem.*, 2004, **25**, 1157-1174.
9. J. Wang, W. Wang, P. A. Kollman and D. A. Case, *J. Mol. Graphics Modell.*, 2006, **25**, 247-260.
10. P. Cieplak, W. D. Cornell, C. Bayly and P. A. Kollman, *J. Comput. Chem.*, 1995, **16**, 1357-1377.
11. Tutorial A1, Amber web site, http://ambermd.org/tutorials/advanced/tutorial1/section1.htm).
12. C. I. Bayly, P. Cieplak, W. Cornell and P. A. Kollman, *J. Phys. Chem.*, 1993, **97**, 10269-10280.
13. R. Ditchfield, W. J. Hehre and J. A. Pople, *J. Chem. Phys.*, 1971, **54**, 724-728.

14. W. J. Hehre, R. Ditchfield and J. A. Pople, *J. Chem. Phys.*, 1972, **56**, 2257-2261.
15. P. C. Hariharan and J. A. Pople, *Theor. Chem. Acc.*, 1973, **28**, 213-222.
16. P. C. Hariharan and J. A. Pople, *Mol. Phys.*, 1974, **27**, 209-214.
17. M. S. Gordon, *Chem. Phys. Lett.*, 1980, **76**, 163-168.
18. M. M. Francl, W. J. Pietro, W. J. Hehre, J. S. Binkley, D. J. DeFrees, J. A. Pople and M. S. Gordon, *J. Chem. Phys.*, 1982, **77**, 3654-3665.
19. R. C. Binning Jr. and L. A. Curtiss, *J. Comput. Chem.*, 1990, **11**, 1206-1216.
20. J.-P. Blaudeau, M. P. McGrath, L. A. Curtiss and L. Radom, *J. Chem. Phys.*, 1997, **107**, 5016-5021.
21. V. A. Rassolov, J. A. Pople, M. A. Ratner and T. L. Windus, *J. Chem. Phys.*, 1998, **109**, 1223-1229.
22. V. A. Rassolov, M. A. Ratner, J. A. Pople, P. C. Redfern and L. A. Curtiss, *J. Comput. Chem.*, 2001, **22**, 976-984.
23. A. D. Becke, *J. Chem. Phys.*, 1993, **98**, 5648-5652.
24. M. J. Frisch, G. W. Trucks, H. B. Schlegel, G. E. Scuseria, M. A. Robb, J. R. Cheeseman, G. Scalmani, V. Barone, B. Mennucci, G. A. Petersson, H. Nakatsuji, M. Caricato, X. Li, H. P. Hratchian, A. F. Izmaylov, J. Bloino, G. Zheng, J. L. Sonnenberg, M. Hada, M. Ehara, K. Toyota, R. Fukuda, J. Hasegawa, M. Ishida, T. Nakajima, Y. Honda, O. Kitao, H. Nakai, T. Vreven, J. A. Montgomery Jr., J. E. Peralta, F. Ogliaro, M. J. Bearpark, J. Heyd, E. N. Brothers, K. N. Kudin, V. N. Staroverov, R. Kobayashi, J. Normand, K. Raghavachari, A. P. Rendell, J. C. Burant, S. S. Iyengar, J. Tomasi, M. Cossi, N. Rega, N. J. Millam, M. Klene, J. E. Knox, J. B. Cross, V. Bakken, C. Adamo, J. Jaramillo, R. Gomperts, R. E. Stratmann, O. Yazyev, A. J. Austin, R. Cammi, C. Pomelli, J. W. Ochterski, R. L. Martin, K. Morokuma, V. G. Zakrzewski, G. A. Voth, P. Salvador, J. J. Dannenberg, S. Dapprich, A. D. Daniels, Ö. Farkas, J. B. Foresman, J. V. Ortiz, J. Cioslowski and D. J. Fox, *Gaussian 09*, Gaussian, Inc.: Wallingford, CT, USA, 2009.
25. S. Miertuš, E. Scrocco and J. Tomasi, *Chem. Phys.*, 1981, **55**, 117-129.
26. S. Miertuš and J. Tomasi, *Chem. Phys.*, 1982, **65**, 239-245.
27. J. L. Pascual-ahuir, E. Silla and I. Tuñon, *J. Comput. Chem.*, 1994, **15**, 1127-1138.
28. M. Cossi, V. Barone, R. Cammi and J. Tomasi, *Chem. Phys. Lett.*, 1996, **255**, 327-335.
29. V. Barone, M. Cossi and J. Tomasi, *J. Chem. Phys.*, 1997, **107**, 3210-3221.
30. E. Cancès, B. Mennucci and J. Tomasi, *J. Chem. Phys.*, 1997, **107**, 3032-3041.
31. B. Mennucci and J. Tomasi, *J. Chem. Phys.*, 1997, **106**, 5151-5158.
32. B. Mennucci, E. Cancès and J. Tomasi, *J. Phys. Chem. B*, 1997, **101**, 10506-10517.
33. V. Barone and M. Cossi, *J. Phys. Chem. A*, 1998, **102**, 1995-2001.
34. M. Cossi, V. Barone, B. Mennucci and J. Tomasi, *Chem. Phys. Lett.*, 1998, **286**, 253-260.
35. V. Barone, M. Cossi and J. Tomasi, *J. Comput. Chem.*, 1998, **19**, 404-417.
36. R. Cammi, B. Mennucci and J. Tomasi, *J. Phys. Chem. A*, 1999, **103**, 9100-9108.
37. M. Cossi, V. Barone and M. A. Robb, *J. Chem. Phys.*, 1999, **111**, 5295-5302.
38. J. Tomasi, B. Mennucci and E. Cancès, *J. Mol. Struct.: THEOCHEM*, 1999, **464**, 211-226.
39. R. Cammi, B. Mennucci and J. Tomasi, *J. Phys. Chem. A*, 2000, **104**, 5631-5637.
40. M. Cossi and V. Barone, *J. Chem. Phys.*, 2000, **112**, 2427-2435.
41. M. Cossi and V. Barone, *J. Chem. Phys.*, 2001, **115**, 4708-4717.

42. M. Cossi, N. Rega, G. Scalmani and V. Barone, *J. Chem. Phys.*, 2001, **114**, 5691-5701.
43. M. Cossi, G. Scalmani, N. Rega and V. Barone, *J. Chem. Phys.*, 2002, **117**, 43-54.
44. M. Cossi, N. Rega, G. Scalmani and V. Barone, *J. Comput. Chem.*, 2003, **24**, 669-681.
45. R. Cammi, *J. Chem. Phys.*, 2009, **131**, 164104.
46. R. Cammi, *Int. J. Quantum Chem.*, 2010, **110**, 3040-3052.
47. G. Scalmani and M. J. Frisch, *J. Chem. Phys.*, 2010, **132**, 114110.
48. F. Lipparini, G. Scalmani, B. Mennucci, E. Cancès, M. Caricato and M. J. Frisch, *J. Chem. Phys.*, 2010, **133**, 014106.
49. M. Caricato, *J. Chem. Theory Comput.*, 2012, **8**, 4494-4502.
50. J. Tomasi, B. Mennucci and R. Cammi, *Chem. Rev.*, 2005, **105**, 2999-3094.
51. H. J. C. Berendsen, J. R. Grigera and T. P. Straatsma, *J. Phys. Chem.*, 1987, **91**, 6269-6271.
52. I. S. Joung and T. E. Cheatham III, *J. Phys. Chem. B*, 2008, **112**, 9020-9041.
53. D. A. Case, R. M. Betz, W. Botello-Smith, D. S. Cerutti, T. E. Cheatham III, T. A. Darden, R. E. Duke, T. J. Giese, H. Gohlke, A. W. Goetz, N. Homeyer, S. Izadi, P. Janowski, J. Kaus, A. Kovalenko, T. S. Lee, S. LeGrand, P. Li, C. Lin, T. Luchko, R. Luo, B. Madej, D. Mermelstein, K. M. Merz, G. Monard, H. Nguyen, H. T. Nguyen, I. Omelyan, A. Onufriev, D. R. Roe, A. Roitberg, C. Sagui, C. L. Simmerling, J. Swails, R. C. Walker, J. Wang, R. M. Wolf, X. Wu, L. Xiao, D. M. York and P. A. Kollman, *AMBER 2016*, University of California, San Francisco, 2016.
54. D. R. Roe and T. E. Cheatham, *J. Chem. Theory Comput.*, 2013, **9**, 3084-3095.
55. VMD web page, http://www.ks.uiuc.edu/Research/vmd/).
56. W. Humphrey, A. Dalke and K. Schulten, *J. Molec. Graphics*, 1996, **14**, 33-38.
57. C. Altona and M. Sundaralingam, *J. Am. Chem. Soc.*, 1972, **94**, 8205-8212.
58. Gatterdam K, Joest EF, Dietz MS, Heilemann M, Tampé R. Super-chelators for advanced protein labeling in living cells. Angew. Chem. Int. Ed. 2018;57:5620–5. doi:10.1002/anie.201800827.